

Sr and O isotope constraints on source and crustal contamination in the high-K calc-alkaline and shoshonitic neogene volcanic rocks of SE Spain

R. Benito ^{a,*}, J. López-Ruiz ^a, J.M. Cebriá ^a, J. Hertogen ^b, M. Doblas ^a,
R. Oyarzun ^c, D. Demaiffe ^d

^a *Departamento de Geología, Museo Nacional de Ciencias Naturales (CSIC), José Gutiérrez Abascal 2, 28006 Madrid, Spain*

^b *Fysico-Chemische Geologie, Universiteit Leuven, 3001 Leuven, Belgium*

^c *Departamento de Cristalografía y Mineralogía, Universidad Complutense de Madrid, 28040 Madrid, Spain*

^d *Laboratoire de Géochimie Isotopique et Géodynamique Chimique, Université Libre de Bruxelles, 1050 Brussels, Belgium*

Received 17 September 1997; accepted 27 November 1998

Abstract

The Neogene volcanic province of SE Spain (NVPS) is characterized by calc-alkaline (CA), high-K calc-alkaline (KCA), shoshonitic (SH), ultrapotassic (UP), and alkaline basaltic (AB) volcanic series. All these series, except the AB, have high LILE/LREE, LILE/HFSE and B/Be ratios and high but variable Sr, Pb and O isotope compositions. The KCA and SH lavas contain metapelitic xenoliths whose mineralogical and chemical composition are typical of anatectic restites. The geochemical characteristics of CA, KCA, SH and UP series suggest that they originated from the lithospheric mantle, previously contaminated by fluids derived from pelagic sediments. Additionally, the presence of restite xenoliths in the KCA and SH lavas indicates some sort of interaction between the mantle-derived magmas and the continental crust. Trace element and isotope modeling for the KCA and SH lavas and the restites, point towards the existence of two mixing stages. During the first stage, the lithospheric mantle was contaminated by 1–5% of fluids derived from pelagic sediments, which produced a fertile source heterogeneously enriched in incompatible elements (particularly LILE and LREE), as well as in ⁸⁷Sr/⁸⁶Sr, without significant modifications of the δ¹⁸O values. In the second stage, the primary melts derived from this metasomatized mantle, which inherited the enrichment in LILE, LREE and ⁸⁷Sr/⁸⁶Sr, interacted with crustal liquids from the Betic Paleozoic basement during their ascent towards the surface. This mixing process caused an increase in δ¹⁸O values and, to a lesser extent, in ⁸⁷Sr/⁸⁶Sr ratios. However, the incompatible trace elements abundances only change slightly, even for high mixing rates, due to their similar concentrations in both components. We suggest the following geodynamic scenario to account for the global evolution of this area: (1) a Late Cretaceous to Oligocene subduction scheme during which mantle metasomatism took place, shortly followed by Upper Oligocene to Lower Miocene continental collision, and (2) a Middle to

* Corresponding author. Fax: +34-91-5644-740; E-mail: mcnr114@mncn.csic.es

Upper Miocene extensional event triggering partial melting of the previously metasomatized mantle and the extrusion of the CA and associated magmas. © 1999 Elsevier Science B.V. All rights reserved.

Keywords: Neogene volcanic province of SE Spain; High-K calc-alkaline rock; Shoshonitic rock; Mantle metasomatism; Crustal contamination

1. Introduction

The Neogene volcanic province of SE Spain (NVPS) lies along the eastern domain of the Betic Ranges, an orogenic edifice built during a series of compressional episodes (Cretaceous to Upper Oligocene–Lower Miocene) leading to nappe stacking and low- to high-grade metamorphism. The plate-tectonic evolution of this realm indicates a long and complex history involving subduction of oceanic crust during Cretaceous to Oligocene time, followed by continental collision and subsequent slab detachment under the Iberian plate in Oligocene time (Vissers and van der Wal, 1993). During Middle to Upper Miocene times, the Betics underwent extensional collapse through low-angle detachment systems involving the rapid unroofing (> 3 km/Ma) of metamorphic core complexes and the extrusion of the NVPS volcanics in a Basin- and Range-type tectonic scenario (Doblas and Oyarzun, 1989; Loneragan and Mange-Rajetsky, 1993; Oyarzun et al., 1995).

The NVPS comprises the following series: calc-alkaline (CA), high-K calc-alkaline (KCA), shoshonitic (SH), ultrapotassic (UP), and alkali basalts (AB) (Fig. 1). The first four series were extruded during Langhian–Messinian, in a time span of 9 Ma, beginning with the CA series in the SE coastal area of Cabo de Gata (15 to 7 Ma), followed inland by the KCA (El Hoyazo, Mazarrón and Mar Menor) and the SH ones (Vera, Mazarrón and Cartagena) (12 to 6 Ma), and finally, the UP series in Vera, Mazarrón and the northern sector of the province (8 to 6 Ma) (Bellon and Brousse, 1977; Nobel et al., 1981; Bellon et al., 1983; Di Battistini et al., 1987). After a gap of 2 Ma, the AB extruded during a second volcanic event. This magmatism is not genetically linked to the previous series and will not be considered here.

The NVPS displays several characteristics which set it apart from comparable volcanic zones associ-

ated with active margins: (1) a whole magmatic suite ranging from CA to UP developed within a narrow area ($\sim 150 \times 25$ km); (2) the plate tectonic setting did not include coeval subduction of oceanic lithosphere; (3) the volcanics have Sr, Nd, Pb and O isotopic ratios higher than those typical of active margins, and (4) most of the NVPS volcanism developed on a relatively thin continental crust (~ 20 km). These unusual conditions call for a new approach regarding the geochemical and geodynamic modeling of the NVPS.

Previous models have explained the NVPS in terms of anatexic melting of metamorphic rocks (Zeck, 1968, 1970; Munksgaard, 1984), mantle metasomatism with sediment-derived fluids (Nelson et al., 1986; López-Ruiz and Wasserman, 1991; Nelson, 1992), and magma mixing or assimilation of crustal rocks (Bellon et al., 1983; Zeck, 1992). However, none of these hypotheses can satisfactorily account for the special petrological and geochemical features exhibited by the KCA and SH rocks which are characterized by the ubiquitous presence of metapelitic xenoliths as well as xenocrysts formed by disaggregation of former inclusions. These characteristics suggest that in addition to the source contamination processes—already proposed for the whole of the NVPS lavas—the KCA and SH magmas have also suffered some interaction with the overlying continental crust at shallow levels.

Here, we summarize the main petrological and geochemical characteristics of the Neogene lavas from the NVPS and the metapelitic xenoliths entrained within the KCA and SH lavas. We then discuss the genesis of the KCA and SH volcanism based on geochemical and geodynamic constraints.

2. Analytical methods

Major elements (Si, Ti, Al, total Fe, Mn, Mg, Ca, K and P) were analyzed by wavelength dispersive

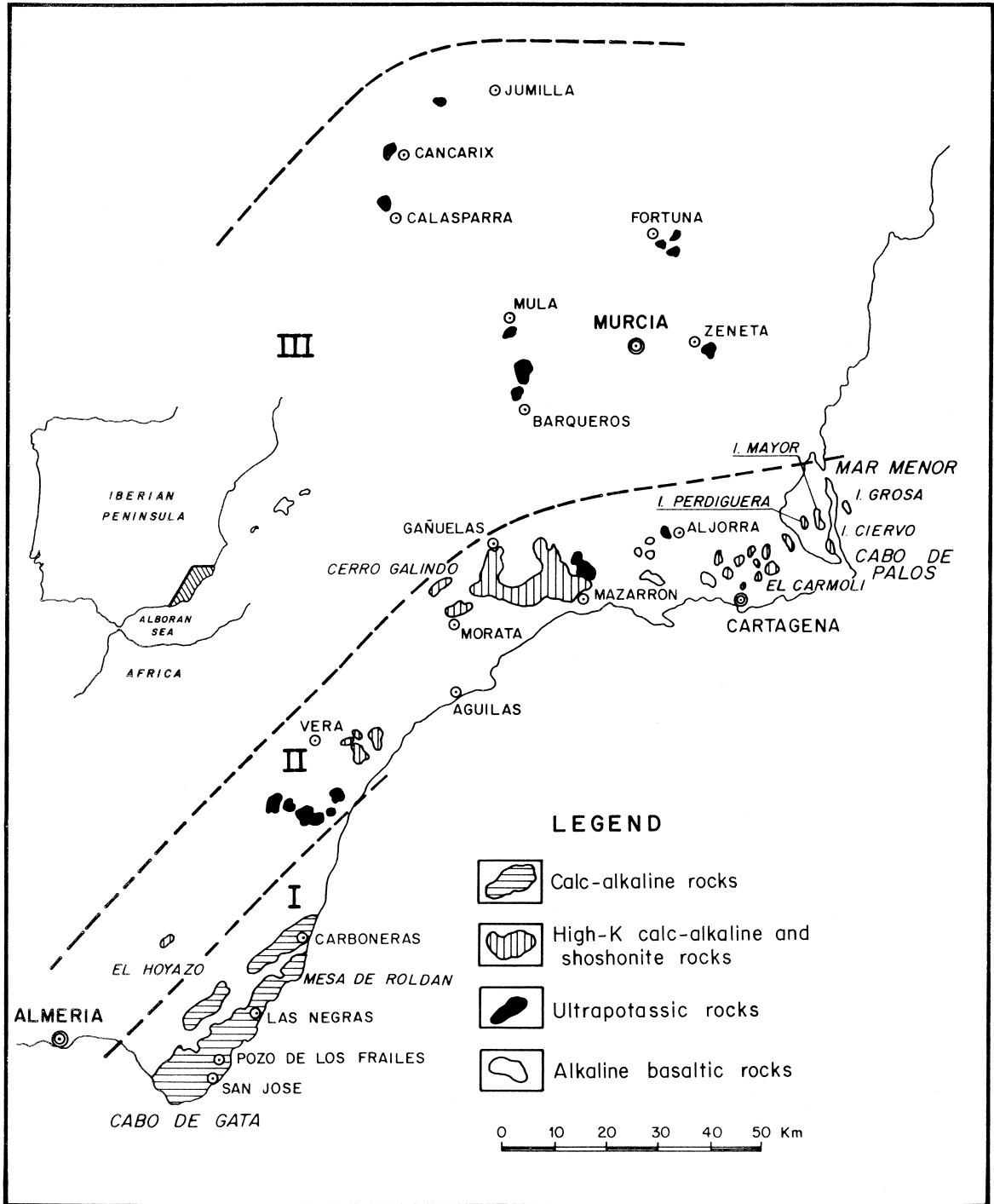


Fig. 1. Sketch of the Neogene volcanic province of SE Spain (NVPS). The dotted lines mark the limit of the zones in which the calc-alkaline (I), high-K calc-alkaline and shoshonitic (II) and ultrapotassic (III) lavas predominate.

X-ray fluorescence (XRF) spectrometry, carried out on an automated Philips PW-1410/20 system, with Cr and W X-ray tubes, at the Museo Nacional de Ciencias Naturales of Madrid (Spain). Analyses were performed using fused glass discs. Undiluted pressed rock powder pellets were used to determine V, Ni, Cu, Rb, Sr, Y, Zr, Nb, Ba and Pb. Natural rock powders were used as standards in each case. The FeO content was analyzed by manganometric titration. The iron content of the xenoliths was analyzed as total Fe (Fe_2O_3^*). Atomic absorption flame spectrometry (Perkin-Elmer-2320) was used to analyze Na and Li over dry digestion with $\text{HNO}_3 + \text{HClO}_4 + \text{HF}$ and HCl extraction. This same digestion was used for determination of Be, analyzed by inductively coupled plasma-atomic emission spectroscopy (Thermo Jarrell Ash, ICAP-61) at the Instituto Tecnológico Geominero de España (Madrid). B was determined also on ICAP-61 over closed digestion with $\text{HClO}_4 + \text{HF} + \text{HCl}$. F was analyzed by colorimetry at this last centre.

Concentrations of Sc, Cr, Co, rare earth elements (REE), Hf, Ta, Pb, Th and U were determined by instrumental neutron activation analysis (INAA) at the University of Leuven (Belgium). The analyses were performed relative to a secondary basalt standard which has been repeatedly calibrated against the BCR-1 reference rock. The experimental errors were of the order of 2%.

Isotopic composition of Sr have been measured by mass spectrometry on double Re filament with a Finnigan MAT-260 mass spectrometer of the Belgian Centre of Geochronology (University of Brussels). Whole-rock samples were dissolved in a $\text{HF}-\text{HNO}_3$ mixture. Strontium was separated by conventional cation exchange techniques. $^{87}\text{Sr}/^{86}\text{Sr}$ ratios are normalized to $^{86}\text{Sr}/^{88}\text{Sr} = 0.1194$. An average $^{87}\text{Sr}/^{86}\text{Sr}$ value of 0.710235 ± 0.000026 is obtained for the NBS-987 standard.

For oxygen isotope measurements, the oxygen was extracted from the whole-rock samples following the general procedure of Clayton and Mayeda (1963), by reaction with BrF_3 and converted to CO_2 for mass spectrometric analysis. O isotopic ratios were measured on a Finnigan MAT-251 spectrometer at the U.S. Geological Survey at Denver (USA). The isotopic data are reported in the conventional δ -notation, where $\delta^{18}\text{O}$ is the relative difference in

isotopic ratio between a sample and SMOW, expressed in parts per thousand. The internal standard used is the NBS-28 reference sample with has a $\delta^{18}\text{O}$ value of +9.6‰. The experimental precision of single determinations is of the order of $\pm 0.2\%$.

3. Petrology and geochemistry of the lavas

The Neogene volcanism of SE Spain has been studied in detail by several authors (e.g., López-Ruiz and Rodríguez Badiola, 1980; Molin, 1980; Munksgaard, 1984; Nixon et al., 1984; Nelson et al., 1986; Venturelli et al., 1984, 1988, 1991, 1993; Toscani et al., 1990, 1995; López-Ruiz and Wasserman, 1991; Zeck, 1992; Benito, 1993; Salvioli and Venturelli, 1996). The general features of this volcanism, as well as detailed petrological and mineralogical descriptions of these rocks (including the criteria followed for their classification), can be found in the above mentioned works and in a more comprehensive way in López-Ruiz and Rodríguez Badiola (1980). In the following sections, only a brief outline of the petrology and geochemistry of the four series is presented.

3.1. Mineralogy

The CA rocks are represented by basaltic andesites, pyroxene- and amphibole-bearing andesites and dacites. The basaltic andesites and the andesites consist of a main assemblage of plagioclase, orthopyroxene, clinopyroxene and magnetite, which can be accompanied by amphibole and biotite in the most silica-rich samples. The dacites are constituted by plagioclase, orthopyroxene, amphibole, biotite, magnetite, ilmenite and quartz.

The KCA series is predominantly corundum-normative high-K andesites and dacites. Although their mineralogy is similar to their equivalents in the CA series, amphibole is never present and biotite is the major ferromagnesian mineral.

The SH series is represented by banakites and latites. The banakites consist of plagioclase (richer in albite and orthoclase than the equivalent rocks of the CA and KCA series), orthopyroxene, clinopyroxene (endiopside–diopside), sanidine, biotite and quartz.

In the latites, plagioclase and sanidine are also coexistent but clinopyroxene is absent and orthopyroxene is scarce, whereas biotite and quartz show higher abundances.

The UP rocks are olivine–diopside–richterite–madupitic lamproites (jumillites), enstatite–sanidine–phlogopite lamproites (cancalites), hyalo-enstatite–phlogopite lamproites (fortunites) and hyalo-olivine–diopside–phlogopite lamproites (verites). In vitreous samples, the glass phase is rich in SiO_2 , Al_2O_3 and K_2O , while in the holocrystalline varieties, it is replaced by potassic richterite and iron-rich sanidine. Apatite, calcite, rutile and spinels are the most important accessory minerals.

3.2. Major and trace elements

Representative chemical analyses of the CA, KCA, SH and UP lavas are selected in Table 1. In Figs. 2 and 3, these series have also been plotted in MgO–element and chondrite-normalized diagrams. In general, the CA rocks are poorer in K_2O , TiO_2 , P_2O_5 and incompatible and compatible trace elements relative to the KCA and SH ones, whereas the UP rocks are richer in K_2O and incompatible trace elements, as well as in MgO, Ni and Cr, relative to the other groups. All the series display the typical signature of lavas belonging to active margins (e.g., $\text{Al}_2\text{O}_3 > 13\%$, $\text{TiO}_2 < 1.2\%$ and high Ba/La, Ba/Nb, La/Nb, Th/Nb, Zr/Nb and B/Be ratios; Perfit et al., 1980; Pearce, 1982; Morris et al., 1990; Hawkesworth et al., 1993, 1994). In this context, it is important to note that all the lavas from the NVPS display a small but persistent negative Eu anomaly as well as a high correlation between $^{87}\text{Sr}/^{86}\text{Sr}$, B and 1/Sr.

The CA rocks exhibit a relatively wide range of SiO_2 and their abundance in major elements is similar to that of equivalent rocks of other areas. They are characterized by high contents of Al_2O_3 and CaO, moderate Na_2O , and low TiO_2 , K_2O and P_2O_5 . This series displays a typical enrichment in LILE (higher in Rb and Th than in Ba) and LREE, and negative anomalies of Sr, Nb, Ta and Ti (Fig. 3). With increasing SiO_2 , a progressive enrichment of K_2O , Rb, Th, Zr and REE is observed, as well as a decrease in Fe_2O_3^* , MgO, CaO, TiO_2 , P_2O_5 , Co, Ni and V.

The KCA rocks show a narrower range of variation in SiO_2 relative to the above described series, but they are usually richer in TiO_2 , K_2O and P_2O_5 , and poorer in FeO and CaO, while Al_2O_3 is similar. They are also enriched in LILE and LREE, and show negative anomalies of Nb, Ta, Sr, P and Ti (Fig. 3). The abundance of all these elements, as well as Ni, Cr, V and Co, is higher than the CA rocks with similar SiO_2 content, but their Ba/La, La/Nb, Th/Nb and Zr/Nb ratios are of the same magnitude. With increasing SiO_2 , Al_2O_3 remains virtually constant, while there is an increase in K_2O and P_2O_5 , and a decrease in MgO and CaO.

In general, the SH rocks are characterized by higher contents of TiO_2 , K_2O and P_2O_5 . They are also strongly enriched in LILE (in this case, the higher values correspond to Th and not to Rb, as in the two other series) and LREE, relative to the rest of incompatible trace elements (Fig. 3). In contrast, their abundance in HREE and compatible elements is in the range observed in the KCA rocks. As a result of the enrichment in highly incompatible elements relative to the moderately incompatible ones, the LILE/LREE and LILE/HFSE ratios are higher than those of the CA and KCA rocks. With increasing silica, Al_2O_3 , MnO, MgO, CaO, TiO_2 and P_2O_5 decrease.

The UP rocks display much higher contents of MgO, Ni and Cr, as well as K_2O , TiO_2 , P_2O_5 , LILE (particularly Th) and LREE, relative to the other groups. On the other hand, they have moderate to low contents of Al_2O_3 , CaO, Sc and V (Figs. 2 and 3)

3.3. Isotopic ratios

The $\delta^{18}\text{O}$ values of the four series range between +9.5 and +20.3‰ (Munksgaard, 1984; López-Ruiz and Wasserman, 1991). There is no good correlation between these values and the abundance of SiO_2 , MgO or incompatible elements. However, there is a strong positive correlation ($r = 0.92$) between $\delta^{18}\text{O}$ and the loss on ignition (LOI) values (Fig. 4). This correlation, as well as the evidence for extensive devitrification of the matrix of many of the samples (which can represent up to > 50% of the rock volume), suggest that the measured $\delta^{18}\text{O}$ values are not primary. The effects of post-crystallization hy-

Table 1
Representative analyses of major (%), trace elements (ppm) and Sr and O isotopes of the lavas from SE Spain

Calc-alkaline lavas						
	Cabo de Gata					
	GAT-7 basaltic andesite	GAT-8 andesite	GAT-18 andesite	GAT-19 andesite	GAT-10 andesite	GAT-11 dacite
SiO ₂	54.47	56.87	60.07	60.71	60.81	63.78
TiO ₂	0.60	0.64	0.40	0.46	0.56	0.51
Al ₂ O ₃	17.93	16.72	16.05	16.14	16.12	15.76
Fe ₂ O ₃	3.25	1.96	1.53	2.12	1.75	1.58
FeO	3.88	5.29	4.63	3.04	4.02	3.42
MnO	0.13	0.13	0.11	0.11	0.11	0.09
MgO	5.55	3.93	4.35	2.40	2.98	2.21
CaO	8.91	8.96	8.35	6.73	7.55	5.90
Na ₂ O	1.16	2.55	1.43	2.12	2.40	2.52
K ₂ O	1.28	1.17	1.15	2.28	1.51	1.85
P ₂ O ₅	0.13	0.14	0.11	0.12	0.10	0.09
LOI	2.31	1.36	1.54	2.70	1.65	2.11
Total	99.60	99.72	99.72	98.93	99.56	99.82
Li	14	14	15	52	27	30
Be	1.1	1.1	1.2	1.6	1.9	1.9
B	31	25	12	20	43	52
F	315	435	270	335	385	505
Sc	–	32.6	31.0	23.7	25.5	20.5
V	210	173	157	104	111	96
Cr	40	90	75	29	81	48
Co	32.0	24.7	19.9	14.8	18.7	13.5
Ni	18	26	13	10	14	8
Cu	21	34	30	13	59	6
Rb	50	33	45	52	73	98
Sr	275	236	218	150	193	204
Y	20	26	17	27	26	27
Zr	115	106	103	105	121	128
Nb	2	2	3	2	6	5
Ba	238	126	272	282	232	244
La	7	11.3	12.1	9.9	14.8	18.8
Ce	31	25.3	24.6	20.7	30.0	38.9
Nd	–	12.2	11.3	8.52	12.6	17.1
Sm	–	3.00	2.52	1.89	2.91	3.34
Eu	–	0.83	0.77	0.58	0.78	0.82
Tb	–	0.51	0.42	0.33	0.49	0.50
Yb	–	1.73	1.65	1.19	1.63	1.68
Lu	–	0.28	0.29	0.22	0.28	0.27
Hf	–	2.03	1.95	1.82	2.55	3.03
Ta	–	0.32	0.38	0.40	0.53	0.59
Pb	17	21	9	14	40	57
Th	5	3.51	3.47	4.62	5.10	6.88
U	–	1.28	0.94	1.90	1.86	2.39
⁸⁷ Sr/ ⁸⁶ Sr	–	–	0.71154	0.71082	0.71298	–
δ ¹⁸ O _{measured}	+11.0	+10.5	+9.5	–	+11.3	+11.6
δ ¹⁸ O _{corrected}	+8.7	+9.9	+8.6	–	+10.2	+9.7

Table 1 (continued)

	Mar Menor		El Hoyazo	Mazarrón
	CAR-1 high-K andesite	CIE-1 high-K andesite	GAT-14 high-K andesite	MAZ-10 high-K dacite
SiO ₂	61.89	62.47	61.44	64.00
TiO ₂	0.59	0.65	0.77	0.58
Al ₂ O ₃	16.70	14.96	17.32	16.02
Fe ₂ O ₃	1.34	0.89	1.29	0.65
FeO	3.37	4.16	3.70	4.09
MnO	0.07	0.09	0.06	0.08
MgO	2.51	2.96	1.95	2.10
CaO	6.18	5.20	3.04	4.83
Na ₂ O	1.76	1.80	1.99	2.48
K ₂ O	2.17	2.22	2.78	2.61
P ₂ O ₅	0.16	0.18	0.14	0.21
LOI	2.85	3.55	4.72	2.49
Total	99.59	99.13	99.20	100.14
Li	20	26	14	33
Be	3	3	4	4
B	63	91	69	57
F	455	415	685	530
Sc	23.8	21.2	17.4	20.7
V	104	126	133	88
Cr	95	208	152	103
Co	11.9	21.3	14.3	12.5
Ni	18	81	29	13
Cu	22	32	32	22
Rb	116	133	90	162
Sr	243	150	334	497
Y	23	20	25	28
Zr	132	139	178	172
Nb	12	12	15	16
Ba	481	350	662	585
La	27.3	26.1	58.1	36.1
Ce	53.1	54.1	104.0	75.4
Nd	24.5	25.6	45.9	34.2
Sm	4.98	4.90	7.92	5.79
Eu	1.08	1.04	1.73	1.30
Tb	0.70	0.72	0.89	0.75
Yb	2.14	2.24	1.78	2.02
Lu	0.31	0.35	0.30	0.27
Hf	3.28	3.64	5.44	4.30
Ta	1.00	0.90	1.38	1.43
Pb	31	21	20	50
Th	10.20	9.65	22.00	21.40
U	4.23	4.53	5.82	8.60
⁸⁷ Sr/ ⁸⁶ Sr	0.71543	0.71563	0.71303	–
δ ¹⁸ O _{measured}	+13.1	+13.2	+17.7	–
δ ¹⁸ O _{corrected}	+9.9	+8.8	+11.1	–

Table 1 (continued)

	Cartagena		Mazarrón			Vera	
	ATA-1 banakite	BEA-1 banakite	MAZ-5 banakite	MAZ-7 latite	MAZ-8 latite	GAR-1 latite	ALI-1 latite
SiO ₂	58.24	59.16	62.88	63.68	64.19	66.62	66.82
TiO ₂	0.73	0.89	0.47	0.71	0.63	0.65	0.64
Al ₂ O ₃	16.25	15.05	14.53	15.53	16.22	15.10	16.09
Fe ₂ O ₃	1.73	1.22	1.03	0.49	0.81	1.87	0.71
FeO	2.91	3.45	3.11	3.54	3.26	1.34	1.55
MnO	0.08	0.07	0.07	0.07	0.05	0.03	0.02
MgO	2.94	3.19	2.31	1.56	1.58	1.77	0.98
CaO	5.50	5.19	2.91	2.71	2.57	2.83	2.39
Na ₂ O	2.12	2.03	1.87	1.74	2.25	1.46	2.33
K ₂ O	4.67	5.15	3.94	4.55	4.43	4.51	3.37
P ₂ O ₅	0.57	0.79	0.36	0.32	0.42	0.65	0.25
LOI	3.94	3.32	6.23	4.69	3.39	3.17	4.00
Total	99.68	99.51	99.71	99.59	99.80	99.73	99.15
Li	–	11	18	18	50	–	26
Be	–	13	4	5	6	–	3
B	–	113	111	112	103	–	56
F	–	1745	795	875	1100	–	990
Sc	19.5	20.9	–	14.6	14	–	11.3
V	98	134	143	108	–	143	94
Cr	132	193	128	97	138	121	87
Co	18.4	16.9	19	11.1	11	25	5.5
Ni	80	75	41	34	49	40	36
Cu	39	51	26	16	18	43	45
Rb	185	339	319	230	227	228	142
Sr	513	624	725	535	581	833	1871
Y	32	31	45	30	31	45	47
Zr	229	339	224	245	260	218	242
Nb	27	35	26	29	33	26	15
Ba	1564	2168	1793	1211	1310	1731	4271
La	62.2	75.6	53	52.4	63.5	43	47.0
Ce	139.0	186.0	91	113.0	137.0	122	106.0
Nd	69.5	106.0	–	54.1	68.2	–	55.0
Sm	11.80	17.90	–	9.47	12.40	–	13.40
Eu	2.31	3.10	–	1.97	2.26	–	2.81
Tb	1.14	1.42	–	1.01	1.18	–	1.90
Yb	2.21	2.14	–	2.33	2.13	–	4.73
Lu	0.31	0.31	–	0.36	0.30	–	0.67
Hf	7.25	10.40	–	6.25	7.67	–	6.49
Ta	2.02	2.62	–	2.25	2.31	–	1.70
Pb	215	90	65	67	71	134	300
Th	67.20	102.00	50	48.70	64.20	48	31.30
U	16.80	26.30	–	16.80	15.40	–	16.70
⁸⁷ Sr/ ⁸⁶ Sr	–	0.71574	–	0.71631	0.71768	–	0.70945
δ ¹⁸ O _{measured}	–	+13.3	+20.3	+15.3	–	+13.4	–
δ ¹⁸ O _{corrected}	–	+9.2	+11.0	+8.7	–	+9.6	–

Table 1 (continued)

Ultrapotassic lavas							
	Jumilla JUM-5 jumillite	Aljorra ALJ-1 verite	Vera VER-4 verite	Cancarix CAN-1 cancalite	Barqueros BAR-1 fortunite	Fortuna FOR-1 fortunite	Salmerón CMO-1 fortunite
SiO ₂	48.99	54.05	55.33	55.33	55.32	55.82	56.88
TiO ₂	1.54	0.91	1.40	1.59	1.63	1.48	1.52
Al ₂ O ₃	8.45	13.35	10.70	9.29	11.24	11.49	9.04
Fe ₂ O ₃	3.94	5.31	0.99	1.89	2.25	2.56	2.29
FeO	1.98	1.09	3.96	3.23	3.40	2.98	2.79
MnO	0.09	0.11	0.08	0.07	0.07	0.08	0.08
MgO	16.68	8.37	11.91	12.97	9.48	19.77	11.56
CaO	7.65	7.28	2.92	3.27	3.59	2.44	3.03
Na ₂ O	1.13	1.39	2.93	0.52	1.25	0.97	1.64
K ₂ O	6.86	5.77	3.48	7.99	6.88	7.93	8.45
P ₂ O ₅	1.25	0.65	0.63	1.09	0.72	0.85	1.08
LOI	1.78	1.74	5.18	2.38	4.46	3.36	1.06
Total	100.34	100.02	99.50	99.62	100.29	99.73	99.42
Li	34	28	67	43	36	45	41
Be	13.5	8.0	11.8	18.2	15.2	14.6	19
B	36	33	238	140	183	113	63
F	3835	1485	3155	3700	3085	4195	5100
Sc	15.5	24.8	13.9	11.7	14.4	13.7	–
V	128	129	139	127	134	111	114
Cr	911	666	722	651	583	561	523
Co	45.2	36.5	37.0	32.6	34.5	33.5	37
Ni	714	392	617	541	479	504	552
Cu	21	46	28	22	29	28	19
Rb	326	265	473	587	500	611	528
Sr	867	466	441	695	516	453	615
Y	31	28	31	33	35	36	32
Zr	538	294	649	727	678	580	856
Nb	54	26	54	57	50	47	68
Ba	2185	1596	1554	1814	1274	1475	1722
La	89.2	68.7	89.5	98.5	84.7	69.2	67
Ce	238.0	173.0	253.0	282.0	248.0	191.0	204
Nd	147.0	104.0	159.0	185.0	163.0	126.0	–
Sm	28.00	18.0	25.60	30.80	26.6	22.60	–
Eu	4.73	3.09	4.22	5.04	4.39	3.78	–
Tb	1.94	1.32	1.53	1.78	1.65	1.54	–
Yb	2.14	1.78	1.67	1.95	2.27	2.19	–
Lu	0.28	0.23	0.20	0.26	0.27	0.30	–
Hf	17.60	9.90	17.80	21.10	19.80	17.60	–
Ta	3.35	2.20	3.26	3.39	3.09	2.78	–
Pb	170	293	205	206	113	75	149
Th	104.00	82.4	90.60	112.00	106.0	85.60	129
U	12.20	16.7	20.20	26.80	22.30	21.30	–
⁸⁷ Sr/ ⁸⁶ Sr	0.71706	0.71974	0.72098	0.71775	0.71810	0.71845	–
δ ¹⁸ O _{measured}	+11.7	+11.4	+18.5	+13.3	–	–	+11.8
δ ¹⁸ O _{corrected}	+10.4	+10.2	+11.1	+10.9	–	–	+11.8

The δ¹⁸O values are from López-Ruiz and Wasserman (1991).

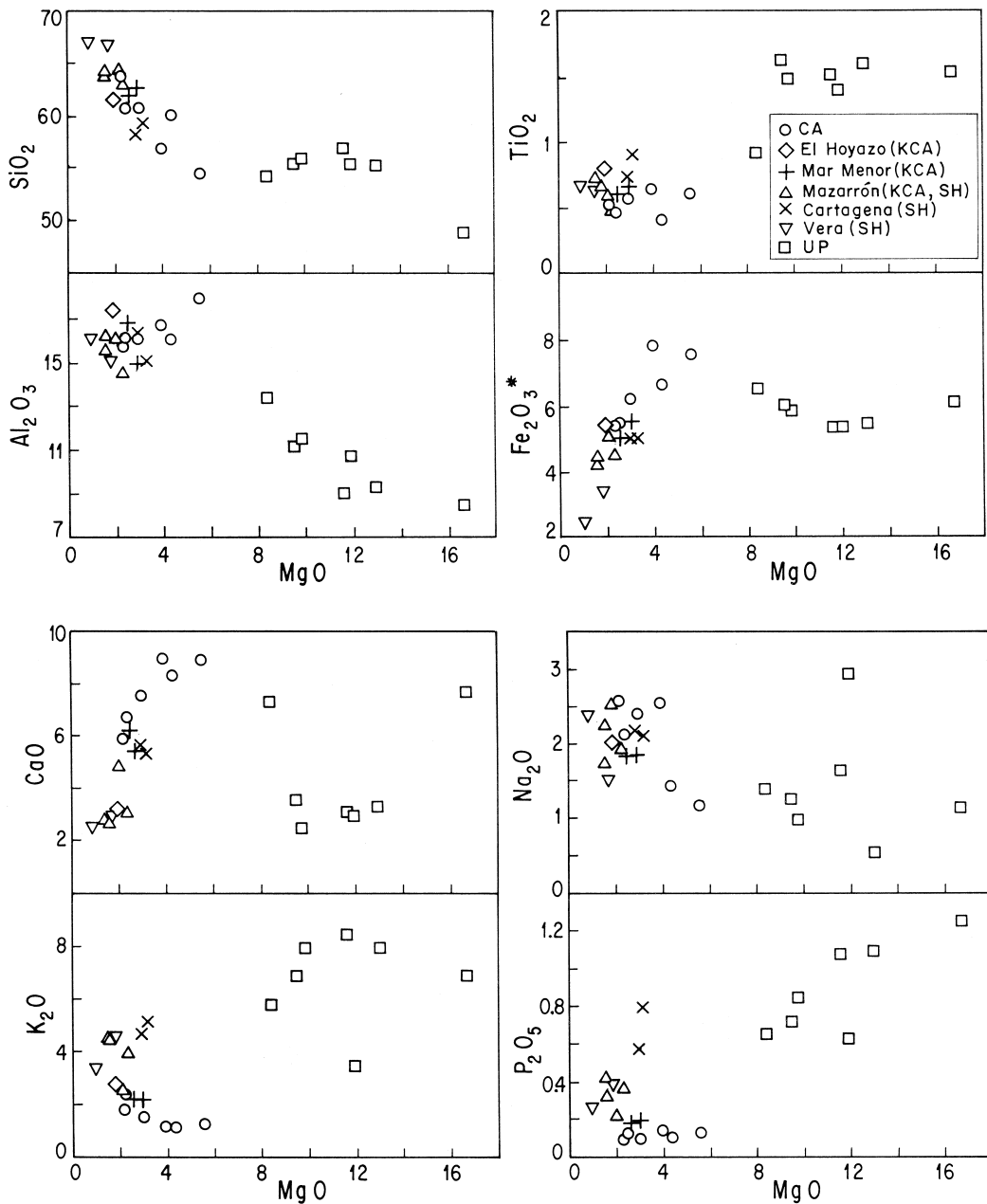


Fig. 2. MgO-major elements diagrams of the calc-alkaline lavas of Cabo de Gata (CA), the high-K calc-alkaline lavas of the El Hoyazo, Mar Menor and Mazarrón (KCA), the shoshonites of Mazarrón, Cartagena and Vera (SH), and the ultrapotassic lavas (UP).

dration and low-temperature alteration on the whole-rock $\delta^{18}\text{O}$ values can be corrected by measuring the $\delta^{18}\text{O}$ values of phenocrysts (e.g., pyroxene) in the lavas or by extrapolation to primary water contents (Ferrara et al., 1985). The pyroxene and

plagioclase phenocrysts of the CA, KCA and SH lavas are usually zoned and the pyroxenes are restricted to the less silicic rocks. For this reason, López-Ruiz and Wasserman (1991) have calculated $\delta^{18}\text{O}$ values corrected for alteration effects following

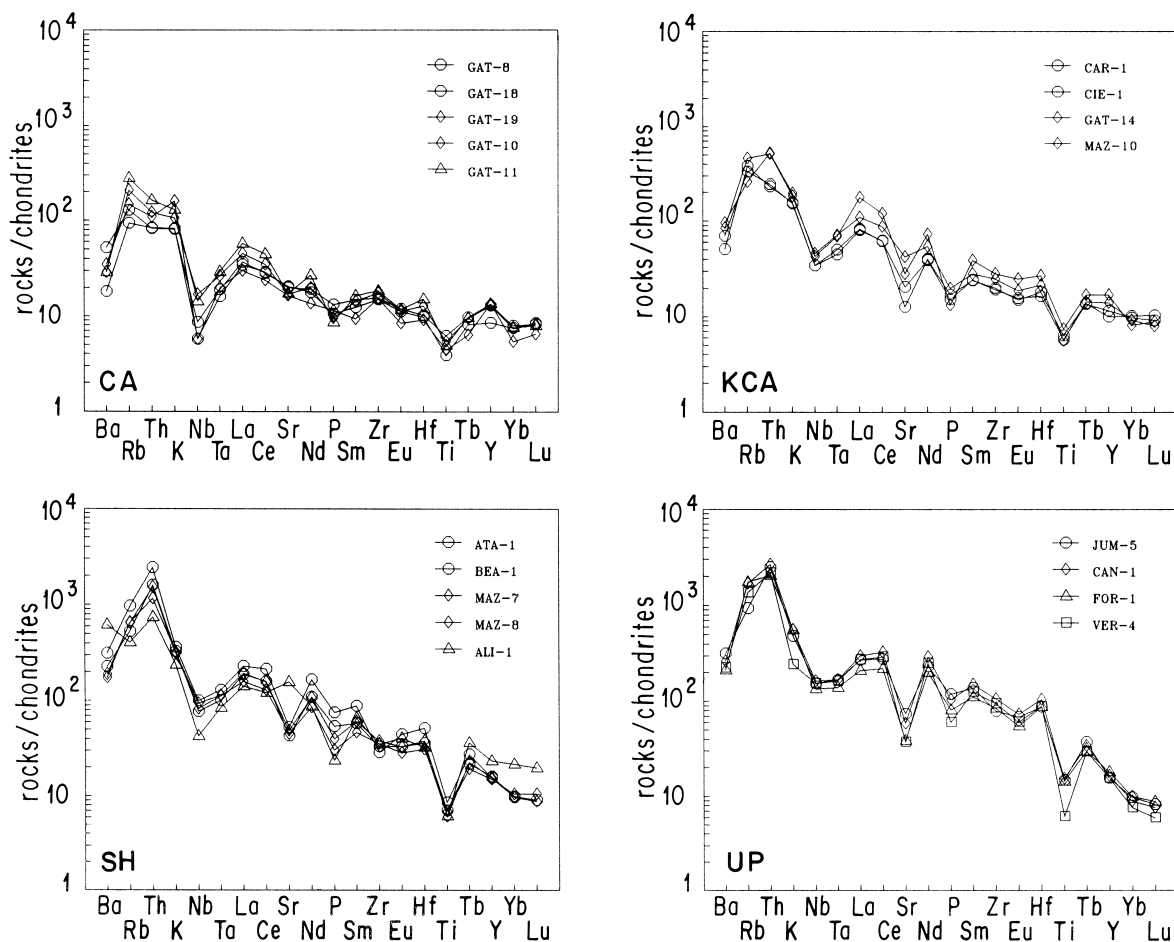


Fig. 3. Multi-element diagrams, normalized with respect to the chondrites, of the calc-alkaline (CA), high-K calc-alkaline (KCA), shoshonitic (SH) and ultrapotassic (UP) lavas of NVPS. The normalization values are the ones suggested by Thompson et al. (1984).

the second method. Although this is an empirical procedure, Ferrara et al. (1985) demonstrated that it can produce results which agree well with those obtained from phenocrysts. The calculated primary values display a much more restricted range (+8.6 to +11.8‰; Table 1 and Fig. 5) with the CA rocks showing lower $\delta^{18}\text{O}$ values (+8.6 to +10.2‰) and the UP ones the highest $\delta^{18}\text{O}$ values (+10.2 to +11.8‰).

The $^{87}\text{Sr}/^{86}\text{Sr}$ ratios in the four series are high (0.7080–0.7213), with a generalized increase from CA to UP, as observed in Fig. 5 (Powell and Bell, 1970; Munksgaard, 1984; Nelson et al., 1986; Toscani et al., 1990; and this work). In contrast to

the oxygen isotopes, the $^{87}\text{Sr}/^{86}\text{Sr}$ ratios have not been significantly modified by alteration processes. This is demonstrated by the Sr isotope analyses performed by Toscani et al. (1990) in whole rock, plagioclase separates and groundmass of CA rocks, which show very small differences, usually within the analytical error. Furthermore, this is supported by the good correlation of the Sr isotopes relative to $^{87}\text{Rb}/^{86}\text{Sr}$ (see Munksgaard, 1984).

Lead isotopic ratios are high in the four series, and there are no significant differences among them. In the CA and UP lavas, $^{206}\text{Pb}/^{204}\text{Pb}$, $^{207}\text{Pb}/^{204}\text{Pb}$ and $^{208}\text{Pb}/^{204}\text{Pb}$ values vary between 18.84 and 18.91, 15.67 and 15.70 and 38.85 and 39.88, and

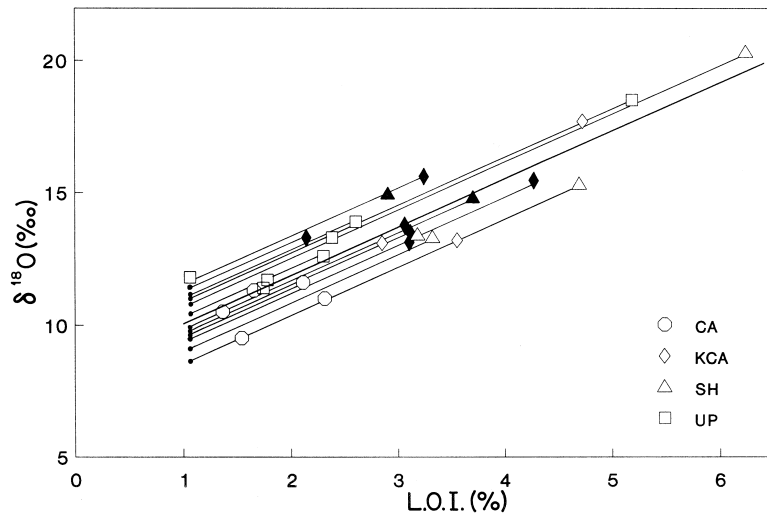


Fig. 4. The $\delta^{18}\text{O}$ -LOI diagram of the calc-alkaline (CA), high-K calc-alkaline (KCA), shoshonitic (SH) and ultrapotassic (UP) lavas of NVPS (open symbols: López-Ruiz and Wasserman, 1991; solid symbols: Munksgaard, 1984). The thick line represents the regression line ($\delta^{18}\text{O} = 1.814 \text{ LOI} + 8.239$) used to correct the obtained data for secondary hydration/devitrification according to the method of Ferrara et al. (1985). The thin lines are extrapolations parallel to the regression line down to a LOI = 1.06%. This value is the total H_2O content of sample CMO-1 which is the only one that is glass-free.

between 18.66 and 18.83, 15.67 and 15.74 and 38.97 and 39.19, respectively (Hertogen et al., 1985, 1988; Nelson et al., 1986; Arribas and Tosdal, 1994).

4. Petrology and geochemistry of the metapelitic xenoliths

The KCA and SH rocks contain two groups of inclusions: metapelitic xenoliths, and igneous

quartz–diorite, basaltoid and quartz–gabbroic inclusions. The first group is more abundant, representing two thirds of the total volume of inclusions. The petrology and chemical composition of both groups of inclusions have been studied by Zeck (1968, 1970, 1992) and Molin (1980).

Metapelitic xenoliths range in diameter from a few millimeters to 50 cm, although most of them are < 10 cm. The disaggregation of these xenoliths pro-

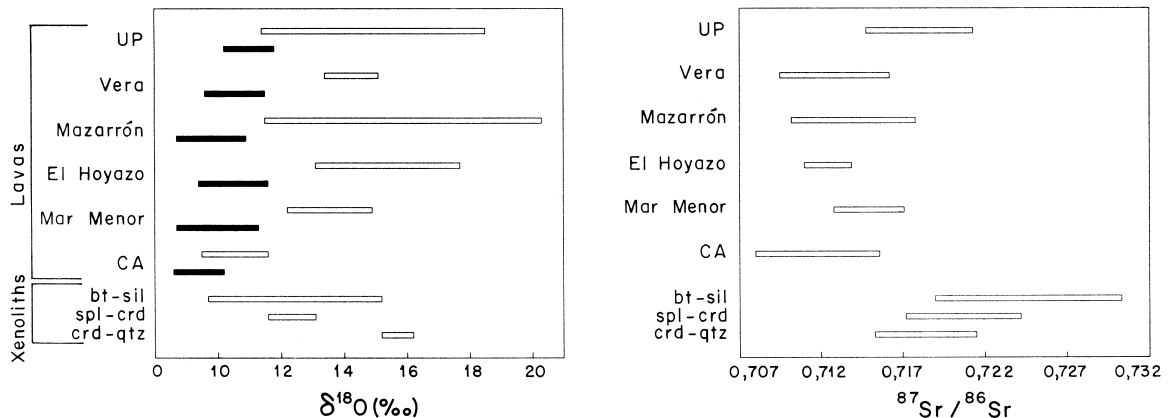


Fig. 5. Sr and O isotopic ratios in the NVPS lavas (after Powell and Bell, 1970; Munksgaard, 1984; Hertogen et al., 1985, 1988; Nelson et al., 1986; Toscani et al., 1990; López-Ruiz and Wasserman, 1991; and this work), and in the gneiss-derived xenoliths of the high-K calc-alkaline and shoshonitic lavas (after Munksgaard, 1984; and this work). In the O isotopes, the open bars correspond to the measured values, while the solid bars represent corrected data.

duced anhedral crystals of cordierite, plagioclase, spinel, zircon and graphite, euhedral garnet crystals, and corroded quartz crystals, which are found within the host lavas. The composition and zoning of the garnet xenocrysts has been studied by López-Ruiz et al. (1977), Molin (1980) and Munksgaard (1985). Here, we will deal with these metapelitic xenoliths, whose textures and mineralogy suggest that they represent refractory residues produced after partial melting episodes from gneisses initially made up of biotite, garnet, sillimanite, feldspars and quartz (Zeck, 1968, 1970; Cesare et al., 1997).

4.1. Mineralogy

The gneissic xenoliths contain biotite and sillimanite which can be accompanied by variable amounts of cordierite, almandine, spinel and quartz. Three main groups of xenoliths can be distinguished according to the relative abundances of those minerals: biotite–sillimanite–almandine (bt–sil–alm), spinel–cordierite (spl–crd) and cordierite–quartz (crd–qtz). These represent end-member terms with a complete transition between them (Zeck, 1968, 1970). Although their distribution is irregular within the volcanic suite, certain types predominate in specific areas. In this sense, the bt–sil–alm types with variable cordierite are the most abundant at El Hoyazo, while the spl–crd ones predominate at Mar Menor.

The mineralogy of these xenoliths suggests that they represent the residue of the original rock assemblage after having lost an anatectic melt fraction. Additionally, the perfect cotectic split into plagioclase-bearing restite without quartz or K-feldspar and quartz-bearing restite without plagioclase or K-feldspar strongly favors an origin by partial melting. The crd–qtz xenoliths probably derive from the comparatively quartz-rich portions of the original gneiss. The inverse ratio of the proportion of cordierite to that of biotite + sillimanite suggests that in the presence of H₂O, quartz and feldspars partially melted at the beginning of the process. Afterwards, during H₂O-free conditions, the reactions responsible for the generation of cordierite would be $bt + sil + qtz = crd + liquid$ or $bt + sil + qtz = crd + K\text{-feldspar} + liquid$, depending on K-feldspar migrating to the liquid or remaining in the xenolith, and $bt + sil = crd + spl + liquid$ (Zeck, 1968, 1970; Benito, 1993).

4.2. Major and trace elements

The bt–sil–alm and the spl–crd xenoliths have similar chemical composition (Table 2). All are Si-poor ($38\% < SiO_2 < 51\%$) and Al-, Fe-, Mg- and Ti-rich ($26\% < Al_2O_3 < 37\%$, $Fe_2O_3 + MgO + TiO_2 = 9\text{--}22\%$). The contents of CaO, Na₂O, MnO and P₂O₅ range between 0.45 and 6.02%, 0.15 and 3.38%, 0.02 and 0.30%, and 0.06 and 0.38%, respectively, depending on the mineralogy. The spl–crd rocks which have lower proportions of biotite, display low concentrations of potassium ($K_2O = 0.25\text{--}2.21\%$), while the biotite-rich xenoliths have higher concentrations ($K_2O = 2.16\text{--}4.69\%$). The crd–qtz rocks show much higher contents of SiO₂ (64.43%), and lower contents of Al₂O₃ (18.37%), CaO (0.43%) and TiO₂ (0.64%) as compared to the above described types.

The bt–sil–alm xenoliths are chemically similar to the average pelites of Taylor and McLennan (1985). However, K₂O and Rb are slightly depleted and Th, Nb, Zr, TiO₂, Ce and La are slightly enriched (Fig. 6). Moreover, the abundance of Ba, Sr, P₂O₅ and Y is highly variable, depending on their content in plagioclase, almandine and apatite. The transition xenoliths between the bt–sil–alm (crd) rocks and the spl–crd ones are characterized by lower Rb concentrations (between 0.2 and 0.7 times the average composition of the pelites), and K₂O, although the abundance of this oxide is variable, depending on their content in biotite. The contents in Th, Nb, Zr, TiO₂, Ce, Y, La, Ba and Sr are high. The spl–crd xenoliths display very high contents of Th, Nb, Zr, TiO₂, Ce, Y and La relative to the pelites. By contrast, K₂O, Rb and Ba are present in very low concentrations. The abundance of Sr and P₂O₅ is variable, and in general, similar to the pelites.

4.3. Isotopic ratios

The ⁸⁷Sr/⁸⁶Sr ratios range between 0.7172 and 0.7303 (Munksgaard, 1984) and the δ¹⁸O values vary between +11.6 and +16.2‰ (Munksgaard, 1984; and this work), except sample ATA-4A (δ¹⁸O = +9.7‰). The ⁸⁷Sr/⁸⁶Sr ratios are higher in the xenoliths than in the host lavas whereas the δ¹⁸O values are similar. However, this similarity is fortu-

itous because the xenolith $\delta^{18}\text{O}$ values are higher than those of the host lava values corrected for hydration/devitrification (Fig. 5).

5. Previous petrogenetic hypotheses

Taking into account the geochemical data of the lavas and their metapelitic xenoliths, we will now

discuss the previous hypotheses for the genesis of the KCA and SH rocks.

5.1. Anatectic melting of metamorphic rocks

The high and homogeneous $\delta^{18}\text{O}$ values of the lavas from El Hoyazo, Vera, Mazarrón and Mar Menor, and of their Al-rich xenoliths, led Munksgaard (1984) to support the hypothesis of Zeck (1968,

Table 2

Representative analyses of major (%), trace elements (ppm) and O isotopes of the gneiss-derived xenoliths

	Mazarrón							
	MAZ-16 bt–sil	MAZ-15 bt–sil	MAZ-14 bt–sil	MAZ-24 bt–sil–crd	MAZ-57A bt–sil–crd	MAZ-20 spl–crd	MAZ-17A spl–crd	MAZ-22 spl–crd
SiO ₂	48.12	49.36	50.33	42.05	47.03	45.29	46.41	47.49
TiO ₂	1.36	1.30	1.40	1.48	1.51	1.64	1.41	1.42
Al ₂ O ₃	26.11	27.69	26.63	33.90	29.73	32.45	31.89	29.49
Fe ₂ O ₃	11.13	7.64	8.38	11.12	8.62	10.37	9.22	9.77
MnO	0.30	0.08	0.13	0.22	0.11	0.08	0.20	0.28
MgO	3.18	1.75	1.73	2.62	2.09	3.67	2.86	2.91
CaO	1.86	1.38	1.73	2.73	3.24	3.21	3.29	2.34
Na ₂ O	1.23	1.95	3.38	1.40	1.77	0.90	1.80	1.61
K ₂ O	4.27	4.25	3.69	1.58	3.30	0.79	1.66	3.06
P ₂ O ₅	0.09	0.15	0.24	0.26	0.13	0.25	0.16	0.10
LOI	2.30	4.31	2.30	2.58	1.39	1.28	0.96	1.08
Total	99.95	99.86	99.94	99.94	98.92	99.93	99.86	99.55
Sc	24.2	24.7	24.6	29.1	25	29	19.3	29
V	237	244	196	270	228	301	249	256
Cr	147	138	119	149	175	193	182	181
Co	15.5	13.5	22.6	19.9	17	16.1	23.6	18.7
Ni	35	48	52	43	30	42	54	42
Cu	10	10	16	52	36	13	27	12
Rb	137	269	162	108	112	33	60	56
Sr	752	389	370	929	722	593	489	513
Y	28	46	33	43	39	43	27	20
Zr	198	247	243	278	343	206	303	411
Nb	–	–	–	–	31	–	–	–
Ba	1916	925	769	1597	1701	475	1078	1045
La	72.7	63.6	51.9	69.3	54	78	75.4	89.2
Ce	153	132	109	145	112	166	155	180
Nd	62.8	57.0	46.1	61.0	–	72.0	67.0	77.0
Sm	11.9	11.1	9.2	11.7	–	13.9	13.2	14.5
Eu	4.69	3.56	2.81	4.68	–	3.67	2.92	3.01
Tb	1.36	1.48	1.28	1.51	–	1.96	1.44	1.48
Yb	4.10	4.49	4.50	5.50	–	4.42	2.51	1.75
Lu	0.59	0.66	0.64	0.81	–	0.64	0.38	0.27
Hf	5.9	7.0	6.9	7.7	–	5.8	8.9	11.5
Ta	1.66	2.05	2.28	1.93	–	2.29	2.59	2.42
Pb	94	81	86	72	87	36	76	80
Th	25.2	21.7	18.1	24.8	24	26.6	28.6	32.4
U	5.7	3.8	5.2	6.8	–	5.3	2.3	6.5
$\delta^{18}\text{O}_{\text{measured}}$	–	–	+15.2	–	+11.9	–	–	+11.6

Table 2 (continued)

	Mar Menor				Cartagena	El Hoyazo	
	MAN-7 spl–crd	MAN-5 spl–crd	MAN-6 spl–crd	CIE-6 spl–crd	ATA-4A bt–sil	GAT-46 bt–sil	GAT-33A crd–qtz
SiO ₂	43.43	44.56	46.37	47.44	47.23	42.05	64.43
TiO ₂	1.80	1.79	1.38	1.74	1.58	1.55	0.64
Al ₂ O ₃	34.82	33.73	34.24	30.70	27.06	29.60	18.37
Fe ₂ O ₃	11.85	10.26	10.95	10.05	8.45	13.47	8.45
MnO	0.17	0.14	0.14	0.17	0.16	0.09	0.08
MgO	2.58	2.24	2.70	1.47	1.77	4.99	3.01
CaO	1.44	3.45	0.96	3.10	6.02	0.55	0.43
Na ₂ O	1.19	1.76	1.02	2.61	2.28	0.15	0.68
K ₂ O	0.31	0.25	1.39	0.52	4.54	2.16	1.27
P ₂ O ₅	0.15	0.21	0.21	0.22	0.25	0.13	0.17
LOI	1.42	1.23	0.92	1.68	0.43	5.06	2.42
Total	99.16	99.62	100.28	99.70	99.77	99.80	99.95
Sc	31.9	31.7	16.1	44	–	16	–
V	341	245	287	301	358	301	112
Cr	213	193	148	182	278	164	110
Co	24.3	22.3	25.6	15	23	17	19
Ni	48	32	37	16	48	37	31
Cu	22	11	11	14	16	14	11
Rb	26	17	41	22	133	113	62
Sr	100	137	35	300	632	53	32
Y	39	52	26	62	48	28	31
Zr	307	374	268	351	334	252	145
Nb	–	–	–	27	–	24	–
Ba	168	162	153	253	928	611	243
La	92.1	81.3	69.3	83	89	43	37
Ce	191	169	142	148	166	84	65
Nd	81.0	73.0	63.0	–	–	–	–
Sm	15.6	14.4	12.4	–	–	–	–
Eu	2.17	2.22	1.23	–	–	–	–
Tb	1.81	1.99	1.49	–	–	–	–
Yb	4.80	5.10	1.98	–	–	–	–
Lu	0.73	0.72	0.30	–	–	–	–
Hf	8.7	10.5	7.6	–	–	–	–
Ta	2.43	2.65	1.98	–	–	–	–
Pb	16	27	21	33	186	11	6
Th	32.6	27.9	23.1	24	26	16	14
U	5.7	5.8	3.9	–	–	–	–
$\delta^{18}\text{O}_{\text{measured}}$	–	–	+12.6	+12.2	+9.7	+15.0	+15.2

1970) that the KCA and SH lavas are derived by anatexis of a (semi-)pelitic rock assemblage. However, as mentioned earlier, the $\delta^{18}\text{O}$ values in the KCA and SH lavas have been strongly modified by secondary alteration and low-temperature hydration/devitrification processes. The pre-alteration $\delta^{18}\text{O}$ values calculated from those of Munksgaard (1984) and López-Ruiz and Wasserman (1991)

are in the range of +8.7 to +11.6‰, which are in general lower than those of the xenoliths. If we also take into account that the $^{87}\text{Sr}/^{86}\text{Sr}$ ratios of the KCA and SH lavas (0.7095–0.7178; Munksgaard, 1984; and this work) are lower than those of the entrained xenoliths (0.7172–0.7303; Munksgaard, 1984), an origin by the partial melting of metamorphic rocks seems unlikely.

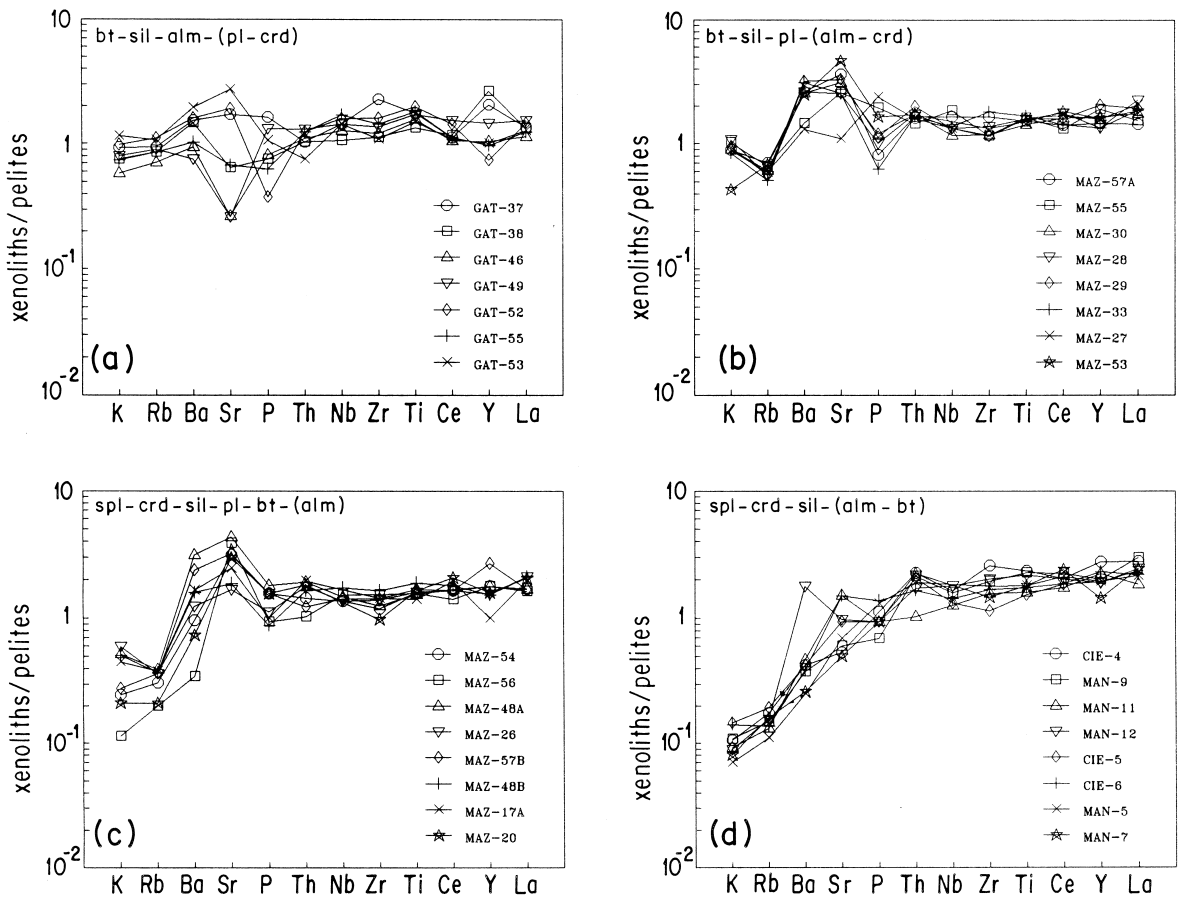


Fig. 6. Trace element variation diagrams, normalized to pelites, of the gneiss-derived xenoliths which are found within the high-K calc-alkaline lavas of El Hoyazo (a) and Mar Menor (d), and within the shoshonites of Mazarrón (b and c). The normalization values correspond to the mean composition of pelites given by Taylor and McLennan (1985).

5.2. Magma mixing or assimilation of crustal materials

According to Zeck (1992), the existence of Al-rich restite, basaltoid and quartz–gabbroic inclusions in the lavas from El Hoyazo suggests that these lavas were generated by mixing/mingling of an anatectic (felsic) melt and a more mafic magma of deeper origin (mantle-derived). When plotted in element-La and element-La/Th diagrams, the volcanic rocks of SE Spain define straight-lines or hyperbolic-curves, depending on the diagram, with the CA and UP rocks plotting at the starting and ending points (Figs. 7 and 8). This suggests a simple two-component mixing process with the KCA and SH lavas being

the result of mixing of CA and UP magmas. However, the major element contents and the Sr and O isotope ratios of the KCA and SH rocks (Figs. 10 and 11) do not follow such mixing trends thus, ruling out this hypothesis.

Alternatively, Bellon et al. (1983) suggested that the assimilation of pelitic material by magmas with characteristics similar to the CA rocks from Cabo de Gata was responsible for the KCA and SH lavas. However, as proposed by Benito (1993), the liquids coming from the metapelitic xenoliths should display concentrations of incompatible trace elements analogous or slightly lower than those of the KCA lavas, and therefore, their mixing with magmas with even lower concentrations in these elements, such as the

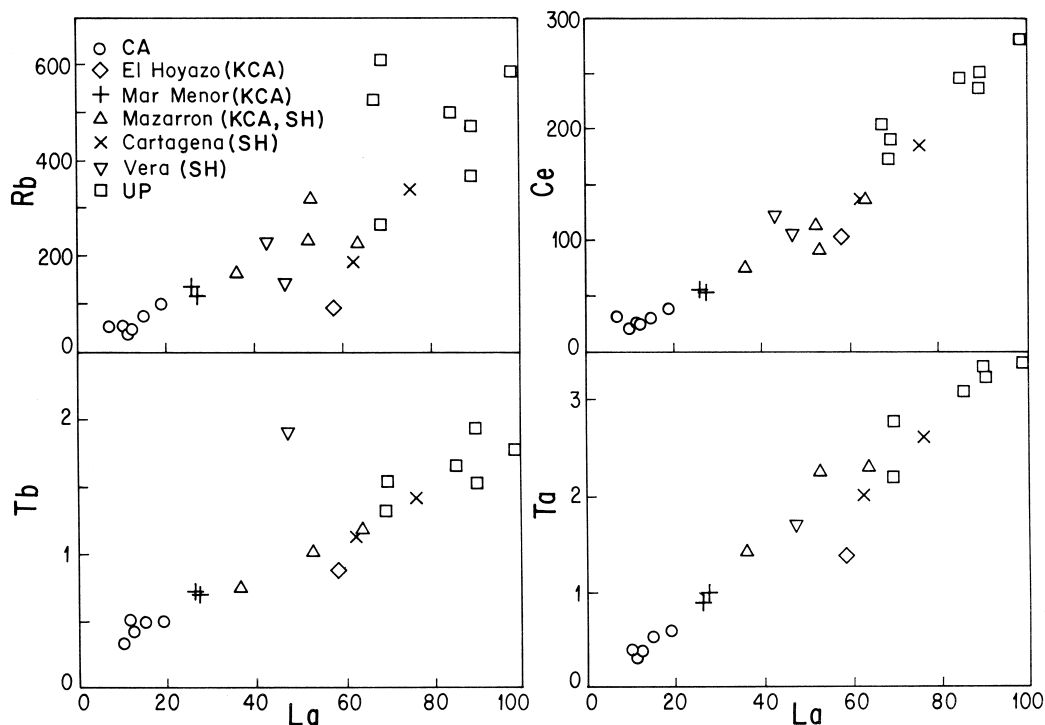


Fig. 7. La–Rb, Ce, Tb, Ta diagrams of the calc-alkaline lavas of Cabo de Gata (CA), the high-K calc-alkaline lavas of the El Hoyazo, Mar Menor and Mazarrón (KCA), the shoshonites of Mazarrón, Cartagena and Vera (SH), and the ultrapotassic lavas (UP).

CA ones, cannot give rise to either the KCA or the SH rocks, which show higher concentrations of these elements.

5.3. Mantle metasomatized with sediment-derived fluids

The distribution of the CA, KCA, SH and UP lavas of SE Spain in the element-La and element-La/Th diagrams (Figs. 7 and 8), as well as their Sr, Pb and O isotopic signature led López-Ruiz and Wasserman (1991) to propose that the four-rock series were derived from a mantle metasomatized by sediment-derived fluids. In element-La diagrams, the liquids resulting from the melting of such a source may show approximately linear trajectories, whenever the degrees of partial melting are similar or proportional to the source-contamination (Fig. 9a). Similarly, in element-La/Th diagrams, the metasomatism of the source is represented by hyperbolic-

curves, and the partial melts derived from it by degrees of melting proportional to the contamination also follow hyperbolic-curves (Fig. 9b). However, the lack of constraints on the trace element contents of the mixing end-members as well as on the bulk solid/liquid distribution coefficients during melting, disallows the calculation of neither the mantle metasomatism trends nor the partial melting parameters. Furthermore, the magmas generated by the combination of these two processes can also be influenced by fractional crystallization and/or crustal contamination. In a $^{87}\text{Sr}/^{86}\text{Sr}$ vs. $\delta^{18}\text{O}$ diagram, the lavas derived from a metasomatized mantle plot along convex-upward hyperbola, as the ratio between the Sr concentration in the mantle and the sediment-derived fluids, is usually lower than 1 (James, 1981). Obviously, if these magmas underwent later assimilation and fractional crystallization, these trajectories would be more or less distorted, depending on the degree of contamination, the composition of the contaminant, and the rate of crystallization.

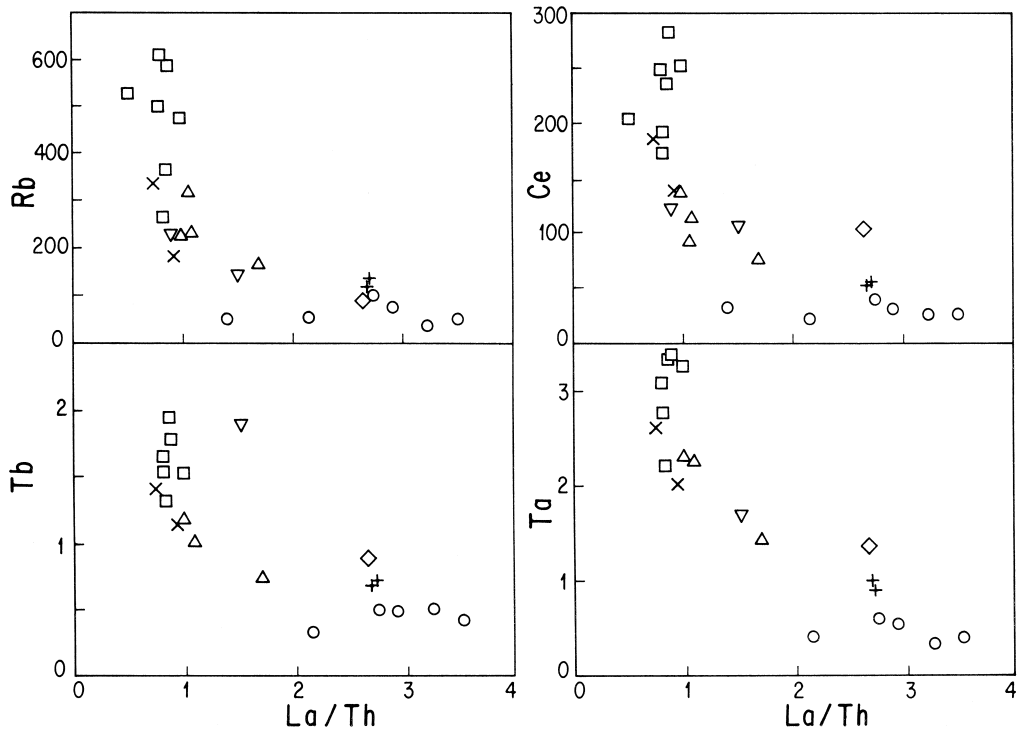


Fig. 8. La/Th–Rb, Ce, Tb, Ta diagrams of the calc-alkaline (CA), high-K calc-alkaline (KCA), shoshonitic (SH) and ultrapotassic (UP) lavas of NVPS. Symbols as in Fig. 7.

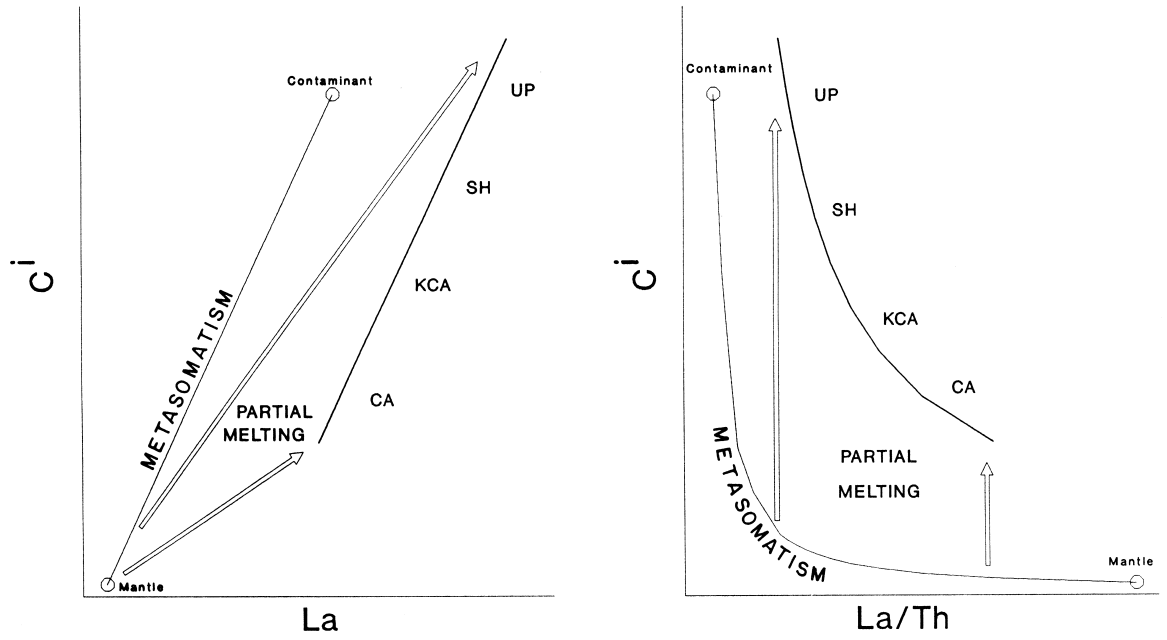


Fig. 9. Theoretical C^i –La and C^i –La/Th diagrams which show the effects of the mantle source contamination through fluids derived from pelagic sediments (metasomatism) and of the partial melting of this source.

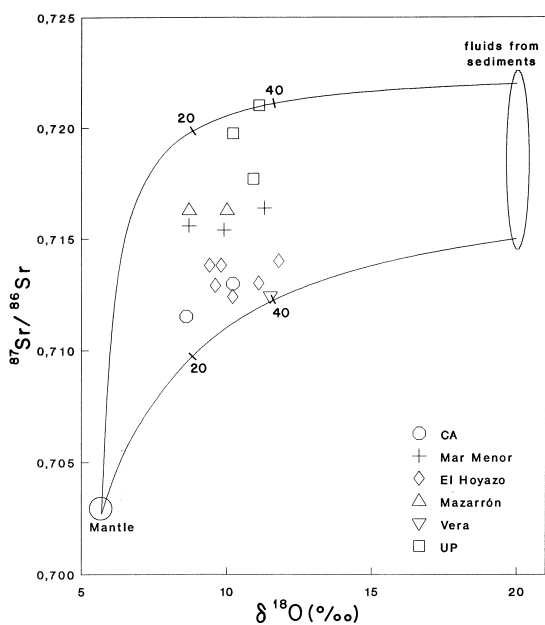


Fig. 10. The $^{87}\text{Sr}/^{86}\text{Sr}$ – $\delta^{18}\text{O}$ diagram of the metasomatism model of the mantle by fluids derived from pelagic sediments, as proposed by López-Ruiz and Wasserman (1991) for the calc-alkaline lavas (CA), the high-K calc-alkaline lavas of the Mar Menor and El Hoyazo, the shoshonites of Mazarrón and Vera, and the ultrapotassic lavas (UP). $^{87}\text{Sr}/^{86}\text{Sr}$ ratios are from Munksgaard (1984) and this work. $\delta^{18}\text{O}$ values are calculated from those obtained by López-Ruiz and Wasserman (1991) and Munksgaard (1984). The numbers next to the metasomatism curves indicate the percentages of participation of the sediment-derived fluids.

According to the hypothesis of mantle metasomatism for the lavas of SE Spain, the mantle component should have low contents of La, Rb, Zr, Ce, Nd, Sm, Eu, Tb, Hf, Ta, U and Th, as well as low Sr and O isotopic ratios, while the one derived from the sedimentary component should have higher contents of these incompatible elements (particularly LILE and LREE) and higher Sr and O isotopic ratios.

In the model proposed by López-Ruiz and Wasserman (1991), it was assumed that the mantle component has a composition equivalent to the depleted lithosphere ($^{87}\text{Sr}/^{86}\text{Sr} = 0.7027$, $\delta^{18}\text{O} = +5.7\text{‰}$ and Sr = 12 ppm). The sediment component corresponds to a fluid derived from subducted pelagic sediments and is highly heterogeneous ($^{87}\text{Sr}/^{86}\text{Sr} = 0.715\text{--}0.722$, $\delta^{18}\text{O} = +20\text{‰}$ and Sr = 60–360 ppm). The compositions located between the two mixing curves represented in Fig. 10 reproduce the isotope

compositions of the CA and associated rocks. However, in this model, the amount of sediment-derived fluids required to explain the high Sr- and O-isotope ratios of the lavas ranges between 20 and 40%.

Although this single-step mixing model can account for the elemental composition and the isotopic ratios of the lavas of SE Spain, and it is probably valid for the UP rocks (Nelson, 1992) and the CA, it does not take into account the obvious interaction of the KCA and SH magmas with the crustal rocks during their ascent to the surface. This model also fails to account for the strong linear correlation shown by some KCA (El Hoyazo and Mar Menor) and SH rocks (Vera) in the $^{87}\text{Sr}/^{86}\text{Sr}$ – $1/\text{Sr}$ diagram (Fig. 11). Moreover, the linear trends displayed by the lavas on this diagram could only be produced in the unlikely situation of a metasomatized mantle source with heterogeneous $^{87}\text{Sr}/^{86}\text{Sr}$ ratios, and where the degrees of melting are inversely proportional to this ratio, in order to generate melts with a

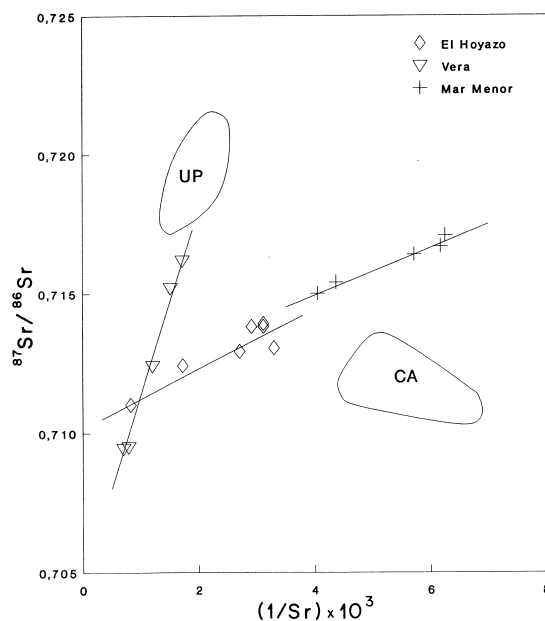


Fig. 11. The $^{87}\text{Sr}/^{86}\text{Sr}$ – $1/\text{Sr} \times 10^3$ diagram for the high-K calc-alkaline lavas of El Hoyazo and Mar Menor (KCA), and shoshonites of Vera (SH). Data are from Munksgaard (1984) and this work. The fields for the calc-alkaline (CA) and ultrapotassic (UP) magmas have been included for comparison. The linear trends observed for the KCA and SH (absent in the CA and UP) are interpreted as the result of mixing.

smaller Sr concentration which correlates with a higher isotopic ratio.

6. A new model: mantle metasomatism + crustal contamination

The distribution of the KCA rocks from El Hoyazo and Mar Menor and the SH from Vera on the $^{87}\text{Sr}/^{86}\text{Sr}-\delta^{18}\text{O}$ and $^{87}\text{Sr}/^{86}\text{Sr}-1/\text{Sr}$ diagrams, suggests a more complex petrogenetic model, which should also be in agreement with the geodynamic frame proposed for this area. In the following paragraphs, we will first test the feasibility of this model from a geochemical point of view and then we will discuss the geodynamic evolution of the area.

6.1. Geochemical modeling

Although mantle metasomatism (as suggested by previous authors and supported by the geodynamic evolution of this region) can account for some of the anomalous geochemical characteristics of the magmas, the distribution of the KCA and SH rocks on the $^{87}\text{Sr}/^{86}\text{Sr}-\delta^{18}\text{O}$ and $^{87}\text{Sr}/^{86}\text{Sr}-1/\text{Sr}$ diagrams and the presence of metapelitic xenoliths suggest that interaction with crustal rocks also played a role. We thus, propose here a two-stage model, involving mantle metasomatism by sediment-derived fluids followed by crustal contamination of the metasomatized mantle-derived magmas. This scenario is similar to those suggested for the island of Martinique in the Lesser Antilles (Davidson and Harmon, 1989) and the Aeolian Islands (Ellam and Harmon, 1990).

To test this model and to establish the values of its parameters, we have assumed as a first approach that the interactions between the different components take place by simple binary mixing, as in this mechanism, the mixing lines join the two end-member compositions. As trace elements alone do not allow to distinguish between partial melting of a metasomatized mantle and crustal contamination, for these calculations, we have considered the variations in $\delta^{18}\text{O}$, $^{87}\text{Sr}/^{86}\text{Sr}$ and Sr. The crustal contamination can also take place by simultaneous assimilation and fractional crystallization (AFC). Additionally, simple fractional crystallization (FC) can occur before and/or after the contamination process. These processes will also be considered later.

6.1.1. Mantle metasomatism

To calculate the trends that define this interaction, it is necessary to assume the composition of the original mantle and the sediment-derived fluids. Due to the lack of additional constraints, we have assumed a depleted lithospheric signature for the starting composition of the mantle ($\delta^{18}\text{O} = +5.7\text{‰}$, $^{87}\text{Sr}/^{86}\text{Sr} = 0.7027$ and Sr = 12 ppm; see, e.g., Ellam and Hawkesworth, 1988; Hart, 1988; Harmon and Hoefs, 1995). For the metasomatizing fluids derived from pelagic sediments, a reasonable $\delta^{18}\text{O}$ value can be $+20\text{‰}$ (Taylor and Sheppard, 1986; Davidson and Harmon, 1989; Ellam and Harmon, 1990). Because the marine sediments have a wide range in Sr (17–1570 ppm; see Dasch, 1969; Biscaye and Dasch, 1971; White et al., 1985; Ben Othman et al., 1989), we assumed an intermediate value (861 ppm; see Biscaye and Dasch, 1971). If the mobility of Sr during dehydration is 41% (Kogiso et al., 1997), the resulting abundance of Sr in the fluids is ~ 360 ppm. As their minimum Sr isotopic ratio is imposed by the maximum of the lavas (0.7213), we have assumed that $^{87}\text{Sr}/^{86}\text{Sr} = 0.722$. This value is within the range shown by marine sediments (0.7021–0.7429; see Dasch, 1969; Biscaye and Dasch, 1971; White et al., 1985; Ben Othman et al., 1989). All these parameters are summarized in Table 3.

The calculated metasomatism curve is a convex-upward hyperbola on the $^{87}\text{Sr}/^{86}\text{Sr}-\delta^{18}\text{O}$ diagram (Fig. 12a) and a straight line with negative slope on the $^{87}\text{Sr}/^{86}\text{Sr}-1/\text{Sr}$ diagram (Fig. 12b). The composition of the metasomatized mantle sources in Mar Menor, El Hoyazo and Vera should be located somewhere along these trends. Obviously, melting of this mantle produces magmas which inherit the isotopic ratios of their sources but not the trace element contents. For this reason, the composition of the primary magmas should plot on the curve of Fig. 12a but not on the line of Fig. 12b. As none of the lavas considered plot on the curve of Fig. 12a, this model implies that all suffered later crustal contamination.

6.1.2. Crustal contamination

The isotopic composition of the crustal liquids can be directly obtained from the high-Al restite xenoliths that are found in these rocks. For calculation purposes, we have considered the average and

Table 3
The $\delta^{18}\text{O}$ values (‰), $^{87}\text{Sr}/^{86}\text{Sr}$ ratios and Sr concentrations (ppm) of the components involved in the mantle metasomatism + crustal contamination process

	Lithospheric mantle	Fluids derived from sediments	Metasomatized mantle			Mantle melts			Crustal liquids		
			Mar Menor	El Hoyazo	Vera	Mar Menor	El Hoyazo	Vera	Mar Menor	El Hoyazo	Vera
$\delta^{18}\text{O}$	+ 5.7	+ 20	+ 6.4	+ 6.1	+ 5.9	+ 6.4	+ 6.1	+ 5.9		+ 14	
										+ 16.2	
$^{87}\text{Sr}/^{86}\text{Sr}$	0.7027	0.7220	0.7145	0.7115	0.7080	0.7145	0.7115	0.7080		0.7220	
										0.7303	
Sr	12	360	29	21	16	300	850	1900	80	100	400
									45	60	270

For data sources (lithospheric mantle and fluids derived from sediments) and calculation procedures, see text.

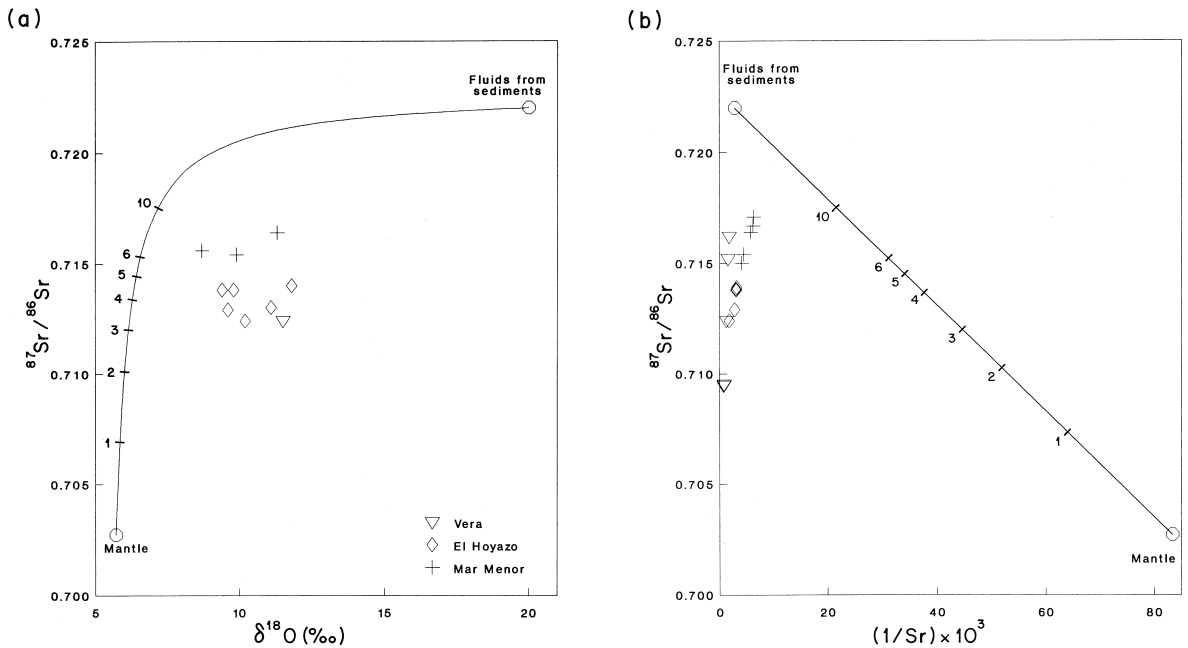


Fig. 12. The $^{87}\text{Sr}/^{86}\text{Sr}-\delta^{18}\text{O}$ (a) and $^{87}\text{Sr}/^{86}\text{Sr}-1/\text{Sr} \times 10^3$ (b) diagrams for the metasomatism of the mantle. $^{87}\text{Sr}/^{86}\text{Sr}$ ratios and Sr concentrations for the lavas are from Munksgaard (1984) and this work. $\delta^{18}\text{O}$ values are calculated from those obtained by López-Ruiz and Wasserman (1991) and Munksgaard (1984). The numbers next to the metasomatism curve indicate the percentages of participation of the sediment-derived fluids.

maximum values of $^{87}\text{Sr}/^{86}\text{Sr}$ (0.7220 and 0.7303, respectively) and $\delta^{18}\text{O}$ (+14‰ and +16.2‰, respectively). The minimum values (0.7172 and +11.6‰) were not considered as they are equal or lower than the maximum for the lavas (0.7178 and +11.6‰). The $^{87}\text{Sr}/^{86}\text{Sr}$ ratios are used to calculate their corresponding Sr concentration by taking into account the regression lines for the lavas on the $^{87}\text{Sr}/^{86}\text{Sr}-1/\text{Sr}$ diagram (Fig. 13; Table 3), which correspond to mixing lines.

The isotopic ratios of the primary mantle-derived magmas are situated on the metasomatism curve of Fig. 12a and the crustal contamination lines are hyperbolae which start at the composition of the initial magmas and finish at the points that represent the crustal liquids. This means that the isotopic ratios of the mantle-derived magmas can be calculated by locating the intersection of both curves on the $^{87}\text{Sr}/^{86}\text{Sr}-\delta^{18}\text{O}$ diagram. To apply this approach, we calculated crustal contamination curves and selected those that better fit the data for each group (see Fig. 14a). To calculate these curves, it is re-

quired to establish the Sr concentration of the mantle-derived melts whose possible values are linked to the $^{87}\text{Sr}/^{86}\text{Sr}$ ratios by the regression lines on the $^{87}\text{Sr}/^{86}\text{Sr}-1/\text{Sr}$ diagram (Fig. 13). The results of this calculation are summarized in Table 3.

The Sr concentrations of the metasomatized mantle sources are easily obtained from the metasomatism line of the $^{87}\text{Sr}/^{86}\text{Sr}-1/\text{Sr}$ diagram (see Fig. 14b) by drawing lines of constant $^{87}\text{Sr}/^{86}\text{Sr}$ (i.e., partial melting lines).

Finally, the percentages of contribution of the sediment-derived fluids are obtained from the metasomatism curve in Fig. 14a, and those of contribution of crustal liquids are obtained by the mixing lines of Fig. 13 (see Table 4).

6.1.3. Discussion of the results

The results of this model suggest that only a small percentage (1–5%) of sediment-derived fluids have pervaded the lithospheric mantle. These values are similar to those obtained for some island-arcs (e.g., Kay et al., 1978; Barreiro, 1983; Hole et al., 1984;

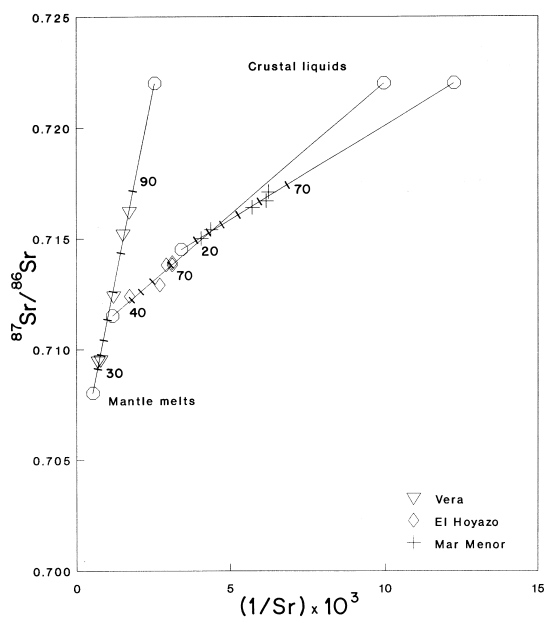


Fig. 13. The $^{87}\text{Sr}/^{86}\text{Sr}-1/\text{Sr} \times 10^3$ diagram of the crustal contamination process for the high-K calc-alkaline lavas of El Hoyazo and Mar Menor, and shoshonites of Vera. The numbers next to the mixing lines indicate the percentages of participation of the crustal liquids. Data source as in Fig. 11.

White and Dupré, 1986; Davidson and Harmon, 1989; Morris and Tera, 1989; Woodhead, 1989; Ellam and Harmon, 1990). The degrees of melting necessary to generate mantle-derived magmas with the calculated Sr concentrations (1900–300 ppm) from the metasomatized mantle with Sr ranging 16–29 ppm are relatively low, even when the residue-melt bulk distribution coefficients for Sr are $\ll 1$ (see Table 4).

If the average value of $^{87}\text{Sr}/^{86}\text{Sr}$ for the restites is assumed to be equivalent to that of the crustal liquids (0.7220), then their proportions of participation during the shallow contamination process range between 22 and 63% at Mar Menor, 36 and 73% at El Hoyazo and 35 and 88% at Vera. However, if the highest $^{87}\text{Sr}/^{86}\text{Sr}$ ratio is considered (0.7303), then the calculated *maximum* participation of the crustal liquids is lower (54%, 70% and 80%, respectively) (Fig. 13; Table 4).

Although these percentages may seem high, even assuming that the crustal liquids had a granitic composition ($\text{SiO}_2 = 66\text{--}71\%$), the primary mantle-derived magmas would have SiO_2 percentages of 46–

57% for the KCA rocks of Mar Menor, 48–57% for the KCA of El Hoyazo and 41–59% for the SH of Vera. These values seem reasonable if we consider that the source has been metasomatized by sediment-derived fluids.

The magmas generated by melting of the metasomatized mantle have higher Sr abundances than those in the crustal liquids. As a consequence, the effect due to crustal contamination in the magmas derived from the metasomatized mantle is to decrease the Sr concentration and to increase the $^{87}\text{Sr}/^{86}\text{Sr}$ and $\delta^{18}\text{O}$ ratios. Concerning the remaining trace elements, as both the KCA/SH lavas and the CA/UP (which have not suffered crustal contamination) follow analogous patterns in the element-La and element-La/Th diagrams (Figs. 7 and 8), it seems plausible that the crustal liquids probably have similar abundances to those in the metasomatized mantle magmas. In this case, crustal contamination only produces slight deviations from the metasomatism + melting curves (Fig. 9). This also explains that in general, the correlation between the Sr isotopic ratios and the trace elements is not high.

In this model, the sediment-derived fluids are mainly responsible for the higher abundance of both the incompatible trace elements and the isotopic ratios of Sr and Pb in the generated magmas. This component is also responsible for the depletion in HFSE, and for the slight negative anomaly of Eu, as these geochemical characteristics are typical of most oceanic sediments (see, e.g., Ben Othman et al., 1989; Lin, 1992; Cousens et al., 1994). Crustal contamination may have contributed to enhance these anomalies, as anatectic melts derived from a metapelitic source usually have these characteristics (Taylor and McLennan, 1985). However, both the CA and UP also have this signature but show no evidences of crustal contamination, thus suggesting that the sediment-derived fluids is the major component controlling the HFSE and Eu anomalies. By contrast, the anatectic melts are mainly responsible for the high $\delta^{18}\text{O}$ values, as they have trace elements concentrations similar to the melts derived from the metasomatized mantle.

6.1.4. Possible effects due to FC and AFC

To avoid assuming many unknown parameters, in Section 6.1.3, high-level differentiation was not con-

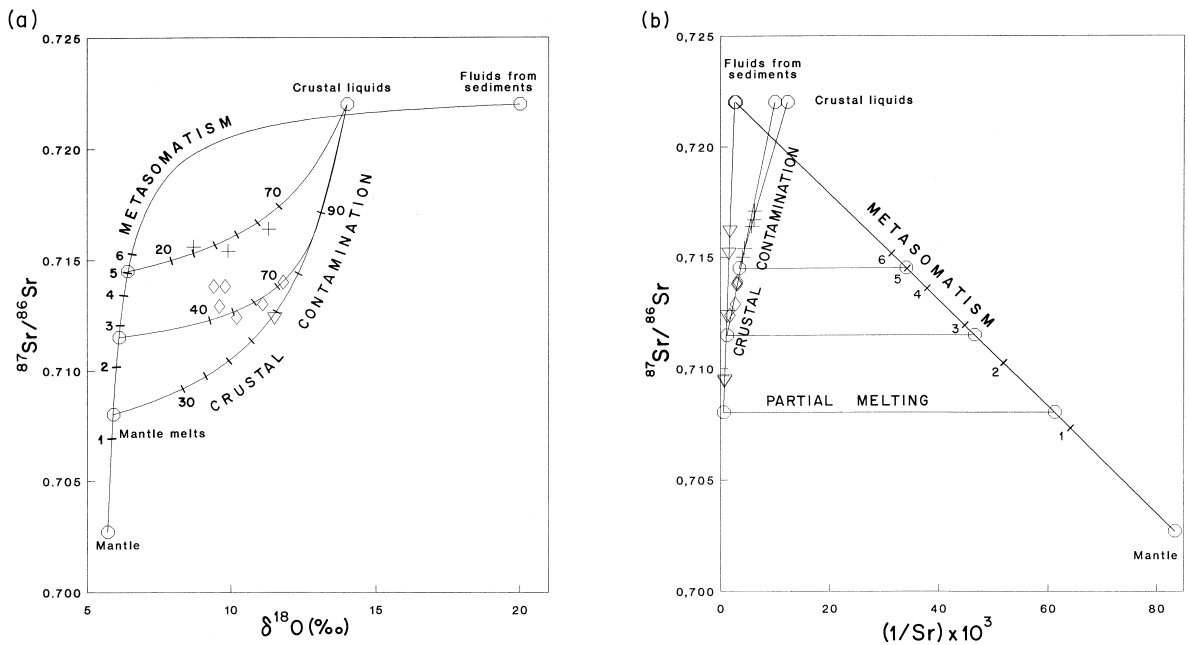


Fig. 14. The $^{87}\text{Sr}/^{86}\text{Sr}-\delta^{18}\text{O}$ (a) and $^{87}\text{Sr}/^{86}\text{Sr}-1/\text{Sr} \times 10^3$ (b) diagrams of the metasomatism of the mantle and crustal contamination model for the high-K calc-alkaline lavas of El Hoyazo and Mar Menor, and shoshonites of Vera. The numbers next to the metasomatism and crustal contamination curve indicate the percentages of participation of the sediment-derived fluids and the crustal liquids, respectively. Data sources as in Fig. 12.

sidered, either before or after the contamination by crustal liquids. If the primitive basaltic partial melts directly derived from the mantle had experienced FC before that contamination, the only variation on the proposed model would correspond to the calculated

melting degrees from the metasomatized mantle. If FC occurred after the contamination, the trends on the $^{87}\text{Sr}/^{86}\text{Sr}-1/\text{Sr}$ diagram would be displaced horizontally when the fractionation rates are identical. The slope of these trends would also be modified

Table 4

Contributions in mixing processes and degrees of partial melting (%) of components involved in the mantle metasomatism + crustal contamination hypothesis

	Metasomatism		Partial melting ($D_{\text{RS}}^{\text{Sr}} = 0.001$)	Crustal contamination ^c	
	Lithospheric mantle	Fluids derived from sediments		Metasomatized mantle	Mantle melts
Mar Menor	95.0	5.0	9.9	37–78 ^a 46–82 ^b	63–22 ^a 54–18 ^b
El Hoyazo	97.3	2.7	2.4	27–64 ^a 30–65 ^b	73–36 ^a 70–35 ^b
Vera	98.8	1.2	0.8	12–65 ^a 20–67 ^b	88–35 ^a 80–33 ^b

^c Calculated using the $^{87}\text{Sr}/^{86}\text{Sr}$ ratios of the restite xenoliths (a: average; b: maximum) and the Sr concentrations calculated for the crustal liquids (see Table 3).

according to the bulk solid/liquid distribution coefficient values. If D^{Sr} is < 1 , the later FC triggers an increased concentration of the Sr in the melts, which is higher when the initial concentration is lower. The contrary situation occurs if D^{Sr} is > 1 . In our case, a value of $D^{Sr} = 0.8$ seems plausible as it would imply the fractionation of 60% plagioclase and 40% orthopyroxene, if we use the distribution coefficients of Gill (1991). These proportions are in agreement with the modal composition of the potassic andesites in the area (López-Ruiz and Rodríguez Badiola, 1980). For example, if the Mar Menor lavas experienced, after the contamination by crustal liquids, a fractionation of 50%, with $D^{Sr} = 0.8$, the initial Sr concentration of the mantle-derived melt would be 240 ppm, and the one of the crustal liquid 75 ppm (Fig. 15a). These concentrations are slightly lower than those calculated for the model without fractionation. As a consequence, the required degree of partial melting of the metasomatized mantle and the crustal contribution would also be lower.

If the crustal contamination follows AFC instead of a simple mixing process, the straight-lines over

the $^{87}Sr/^{86}Sr-1/Sr$ diagram would start at the initial magma composition, but they would not end at the Sr composition of the assimilated material, but at higher values if $D^{Sr} < 1$ or lower ones if $D^{Sr} > 1$. In this case, in addition to D^{Sr} , it is also necessary to assume values for r (ratio of mass of crystals accumulated to the mass of material assimilated; see Taylor, 1980; DePaolo, 1981; Taylor and Sheppard, 1986). For example, if the Mar Menor lavas underwent an AFC process, where $r = 1.25$ and $D^{Sr} = 0.8$, the Sr concentration in the crustal liquid would be 65 ppm (Fig. 15b), lower than those calculated for the simple mixing model.

As it can be deduced from these calculations, to model the effects due to AFC, it would be necessary to assume the values of both D^{Sr} and r thus, introducing higher uncertainties into the model. Finally, it is important to note that independently of the particular process considered to calculate the interaction with crustal components (i.e., AFC vs. simple mixing) and the degree of complexity introduced into the model (i.e., considering the effects due to FC), the general model involving two mixing stages

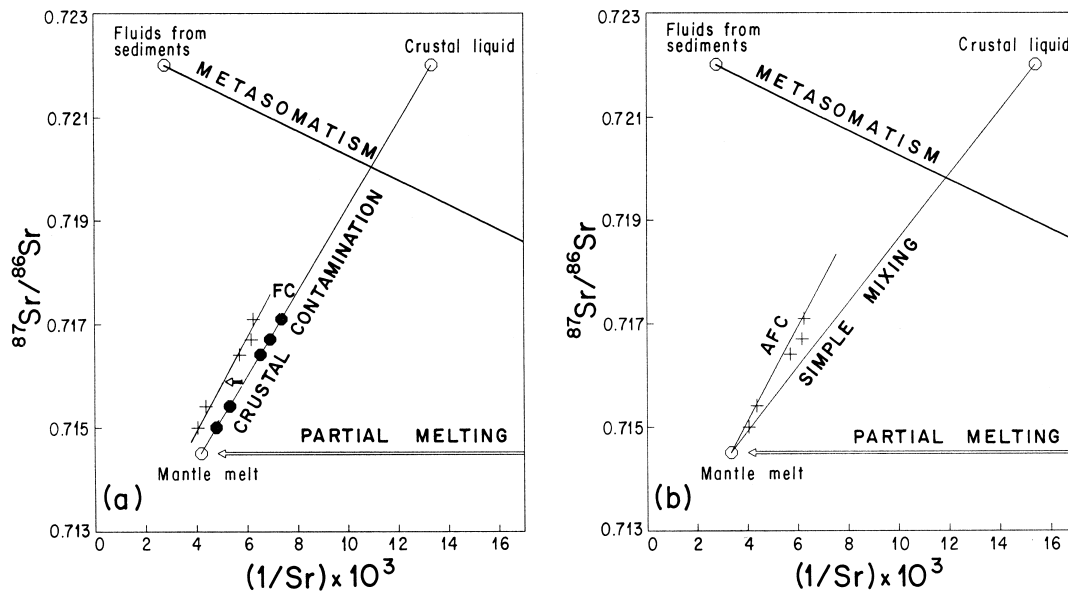


Fig. 15. The $^{87}Sr/^{86}Sr-1/Sr \times 10^3$ diagrams for the high-K calc-alkaline lavas of the Mar Menor. In this diagram, the following situations have been considered: (a) the metasomatized mantle melts have suffered fractional crystallization (FC) after the crustal contamination process, and (b) fractional crystallization and assimilation have been simultaneous (AFC). The crosses represent the lavas (Munksgaard, 1984; and this work) and the solid circles represent the calculated melts.

remains valid, and the only variations would be obtained for the absolute values of the parameters.

6.2. Geodynamic setting

The origin of the NVPS magmas has to be understood in terms of the complex tectonic history of this Alpine realm. The tectonic evolution of the Betics that ultimately led to magmatic activity along the NVPS can be summarized in three main steps (Doblas and Oyarzun, 1989; Banda et al., 1993; Vissers and van der Wal, 1993; Oyarzun et al., 1995): (1) Cretaceous to Oligocene NW-directed subduction of oceanic crust; (2) Upper Oligocene–Lower Miocene continental collision, cessation of subduction, and slab detachment and sinking into the mantle; and (3) Middle to Upper Miocene extensional collapse of the already overthickened orogenic wedge and the onset of magmatic activity along the NVPS (Fig. 16). Asymmetric extension occurred along NE-oriented and SE-dipping major detachment systems. Top-to-the-SE displacement of the upper plate generated the extensional disruption of this realm, involving crustal upward arching, denudation of the Nevado–Filábride metamorphic core complex, and upwelling of the previously metasomatized mantle beneath southeastern Iberia. Within this scenario, volcanism extruded along the NVPS through high-angle normal faults, disrupting the brittle upper-plate of the detachment systems. The overall collapse through major extensional detachment faults resulted in the strong thinning of the Betics realm, within a Basin and Range type tectonic scenario. Geophysical data (IGME, 1983) indicate crustal thinning from 38 km in the Iberian foreland to 14 km within the Alboran Sea. Moho depths beneath the NVPS range between 23 and 30 km (Banda et al., 1993). These values are intermediate between those of a thickened continental margin (50–70 km, Andean Central Volcanic Zone) and the average oceanic crust (7 km). However, since this realm underwent crustal thickening during Pliocene time (López-Ruiz et al., 1993), the current Moho depth of the NVPS might represent a maximum value. Perhaps a crustal thickness of ~20 km would be closer to the actual values for Middle to Upper Miocene times.

As deduced from hot-spot motion (Duncan, 1981), fast N drift of the African plate took place between

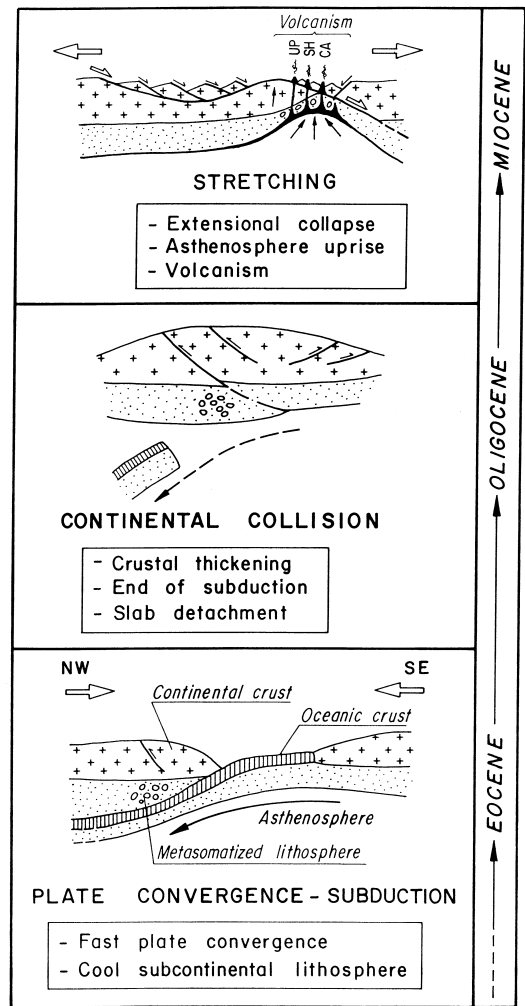


Fig. 16. Schematic model for the Eocene to Miocene geodynamic evolution of SE Spain.

40 and 20 Ma (Upper Eocene–Lower Miocene), thus implying high rates of convergence between Africa and Iberia. Under these conditions, we can envisage a shallow-dipping Benioff zone and an overall compressional stress regime preventing volcanic activity in the Iberian margin (e.g., Barazangi and Isacks, 1979; Jordan et al., 1983). Low-angle subduction would have also implied depression of the mantle isotherms resulting from the introduction of a cool oceanic plate (e.g., Tökösz et al., 1971; Schubert et al., 1975; Anderson et al., 1992). This is further supported by the absence of magmatism during this

period of time (López-Ruiz and Rodríguez Badiola, 1980; Doblas and Oyarzun, 1989). The subsequent extensional collapse of the overthickened Betic orogen through SE-dipping detachment systems induced the following: major lithospheric stretching, asymmetric isostatic uplift of asthenospheric mantle towards the low-pressure thinned region (Doblas and Oyarzun, 1989), melting of the subcontinental lithosphere and Middle to Upper Miocene magmatism along the NVPS. The evolution of the detachment systems gave rise to a NW-dipping/deepening crust–mantle boundary (Fig. 16) which accounts for the NE-oriented geochemical, petrological and age polarity zonation observed within the NVPS (from the SE to NW; Fig. 1), with progressively younger volcanic ages, and a transition from CA to shoshonitic and final lamproitic magmatism (Figs. 1 and 16).

Two main points can be extracted from the previous discussion, which are in agreement with the proposed geochemical model: (1) the existence of a previous subduction under the Betics, and (2) the contemporaneous character of the later extension and magmatism. Subduction processes are likely to have induced a continuous metasomatism of the subcontinental lithosphere by fluids involving a component derived from the sediments carried by the descending slab.

7. Conclusions

The KCA and SH rocks of the NVPS show similarly to the associated CA and UP ones, high LILE/LREE, LILE/HFSE and B/Be ratios and high Sr and O isotope values. Additionally, they entrain metapelitic xenoliths, whose mineralogical and chemical composition suggest that they represent anatectic restites.

The contamination of the lithospheric mantle by a fluid component derived from pelagic sediments provides the geochemical modification of the mantle source necessary to produce the characteristic subduction signature of high LILE/HFSE ratios and isotopic ratios (relative to MORB). However, this hypothesis does not take into account the obvious interaction with crustal rocks experienced by the KCA and SH magmas during their ascent to the surface, as shown by the gneiss-derived xenoliths

which are found within these rocks, nor does it explain the linear trends shown by the KCA and SH rocks in the $^{87}\text{Sr}/^{86}\text{Sr}-1/\text{Sr}$ diagram.

Trace elements and Sr–O isotopic ratios modeling for the KCA and SH lavas, and their restitic xenoliths, allow us to propose a petrogenetic model consisting of two mixing stages. During the first episode, source-contamination (metasomatism) takes place within the lithospheric mantle by fluids derived from subducted pelagic sediments (between 1 and 5%). This process would yield a heterogeneous source enriched in incompatible elements (specially LILE and LREE), and $^{87}\text{Sr}/^{86}\text{Sr}$, with only minor modification of the $\delta^{18}\text{O}$ values. The partial melting of this metasomatized mantle gives rise to magmas highly enriched in LILE and LREE, that inherit the isotopic signature of their source. In the second stage, during their ascent to the surface, these magmas interacted with crustal liquids from the Betic Paleozoic basement. Mixing between these two liquids produced magmas enriched in $\delta^{18}\text{O}$ and to a lower extent in $^{87}\text{Sr}/^{86}\text{Sr}$. On the contrary, although the crustal contribution is high (> 18% at Mar Menor, > 35% at El Hoyazo and > 33% at Vera), the effect on the trace elements abundances is minor due to the similar trace element composition of both crustal- and mantle-derived liquids.

The CA and associated volcanism of SE Spain is atypical in that it is not coeval with subduction processes and it is rather the consequence of the Neogene extensional disruption of a previously enriched lithosphere. Compressional tectonics were active in the Betic orogen during two time-spans: late Cretaceous to Oligocene (subduction) and late Oligocene to early Miocene (continental collision). Therefore, the metasomatism of the lithospheric mantle takes place between the end of the Cretaceous and the beginning of the Miocene, while the crustal contamination and magmatic extrusion occurred during the Middle to Upper Miocene.

Acknowledgements

Financial support was provided by the Dirección General de Enseñanza Superior e Investigación Científica (Spain) through the research project PB95-0107. Sc, REE, Hf, Ta, Th and U, and Sr isotope

analyses were funded in part by the Belgian National Fund for Scientific Research (grants to J.H. and D.D.). We also thank Dr. S. Foley, Dr. A. Embey-Isztin and an anonymous reviewer for their comments on the manuscript.

References

- Anderson, D.L., Zhang, Y.S., Tanimoto, T., 1992. Plume heads, continental lithosphere, flood basalts and tomography. In: Sorey, B.C., Alabaster, T., Pankhurst, R.J. (Eds.), *Magmatism and the Causes of Continental Break-up*, Vol. 68. Geol. Soc. London Spec. Publ., pp. 99–124.
- Arribas, A., Tosdal, R.M., 1994. Isotopic composition of Pb in ore deposits of the Betic Cordillera, Spain: origin and relationship to other European deposits. *Econ. Geol.* 89, 1074–1093.
- Banda, E., Gallart, J., García Dueñas, V., Dañoibeitia, J.J., Makris, J., 1993. Lateral variation of the crust in the Iberian Peninsula: new evidence from the Betic Cordillera. *Tectonophysics* 221, 55–66.
- Barazangi, M., Isacks, B., 1979. Subduction of the Nazca plate beneath Peru: evidence from spatial distribution of earthquakes. *Geophys. J. R. Astron. Soc.* 57, 537–555.
- Barreiro, B.A., 1983. Lead isotopic compositions of South Sandwich Island volcanic rocks and their bearing on magma genesis in intra-oceanic arcs. *Geochim. Cosmochim. Acta* 47, 817–822.
- Bellon, H., Brousse, R., 1977. Le magmatisme périméditerranéen occidental. *Essai de synthèse*. *Bull. Soc. Geol. (France)* 19, 469–480.
- Bellon, H., Bordet, P., Montecat, C., 1983. Chronologie du magmatisme néogène des Cordillères Bétiques, Espagne méridionale. *Bull. Soc. Geol. (France)* 25, 205–217.
- Benito, R., 1993. Hibridación del manto y asimilación de corteza continental en el magmatismo calco-alkalino y shoshonítico del SE de España. PhD Thesis, UAM, 222 pp.
- Ben Othman, D., White, W.M., Patchett, J., 1989. The geochemistry of marine sediments, island arc magma genesis, and crust–mantle recycling. *Earth Planet. Sci. Lett.* 94, 1–21.
- Biscaye, P.E., Dasch, E.J., 1971. The rubidium, strontium, strontium–isotope system in deep-sea sediments: Argentine basin. *J. Geophys. Res.* 76, 5087–5096.
- Cesare, B., Salvioli, E., Venturelli, G., 1997. Crustal anatexis and melt extraction during deformation in the restite xenoliths at El Joyazo, SE Spain. *Mineral. Mag.* 61, 15–27.
- Clayton, R.N., Mayeda, T.K., 1963. The use of bromine pentafluoride in extraction of oxygen from oxides and silicates for isotopic analysis. *Geochim. Cosmochim. Acta* 27, 43–52.
- Cousens, B.L., Allan, J.F., Gorton, M.P., 1994. Subduction-modified pelagic sediments as the enriched component in back-arc basalts from the Japan Sea: Ocean Drilling Program Sites 797 and 794. *Contrib. Mineral. Petrol.* 117, 421–434.
- Dasch, E.J., 1969. Strontium isotopes in weathering profiles, deep-sea sediments, and sedimentary rocks. *Geochim. Cosmochim. Acta* 33, 1521–1552.
- Davidson, J.P., Harmon, R.S., 1989. Oxygen isotope constraints on the petrogenesis of volcanic arc magmas from Martinique, Lesser Antilles. *Earth Planet. Sci. Lett.* 95, 255–270.
- DePaolo, D.J., 1981. Trace elements and isotopic effects of combined wallrock AFC. *Earth Planet. Sci. Lett.* 53, 189–202.
- Di Battistini, G., Toscani, L., Iaccarino, S., Villa, I.M., 1987. K/Ar ages and the geological setting of calc-alkaline volcanic rocks from Sierra de Gata, SE Spain. *Neues Jahrb. Mineral. Mh.* 8, 369–383.
- Doblas, M., Oyarzun, R., 1989. Neogene extensional collapse in the western Mediterranean (Betic–Rift orogenic belt): implications for the genesis of the Gibraltar Arc and magmatic activity. *Geology* 17, 430–433.
- Duncan, R., 1981. Hot-spots in the southern oceans—an absolute frame of reference for motion of the Gondwana continents. *Tectonophysics* 74, 29–42.
- Ellam, R.M., Harmon, R.S., 1990. Oxygen isotope constraints on the crustal contribution to the subduction-related magmatism of the Aeolian islands, southern Italy. *J. Volcanol. Geotherm. Res.* 44, 105–122.
- Ellam, R.M., Hawkesworth, C.J., 1988. Elemental and isotopic variations in subduction related basalts: evidence for a three-component model. *Contrib. Mineral. Petrol.* 98, 72–80.
- Ferrara, G., Laurenzi, M.A., Taylor, H.P., Tonarini, S., Turi, B., 1985. Oxygen and strontium isotope studies of K-rich volcanic rocks from the Alban Hills, Italy. *Earth Planet. Sci. Lett.* 75, 13–28.
- Gill, J.B., 1991. *Orogenic andesites and plate tectonics*. Springer, Berlin, 390 pp.
- Harmon, R.S., Hoefs, J., 1995. Oxygen isotope heterogeneity of the mantle deduced from global ^{18}O systematics of basalts from different geotectonic settings. *Contrib. Mineral. Petrol.* 120, 95–114.
- Hart, S.R., 1988. Heterogeneous mantle domains: signatures, genesis and mixing chronologies. *Earth Planet. Sci. Lett.* 90, 273–296.
- Hawkesworth, C.J., Gallagher, K., Hergt, J.M., McDermott, F., 1993. Mantle and slab contributions in arc magmas. *Annu. Rev. Earth Planet. Sci.* 21, 175–204.
- Hawkesworth, C.J., Gallagher, K., Hergt, J.M., McDermott, F., 1994. Destructive plate margin magmatism: geochemistry and melt generation. *Lithos* 33, 169–188.
- Hertogen, J., López-Ruiz, J., Rodríguez Badiola, E., Demaiffe, D., Weis, D., 1985. Petrogenesis of ultrapotassic volcanic rocks from SE Spain: trace elements and Sr–Pb isotopes. *Terra Cognita* 5, 215–216.
- Hertogen, J., López-Ruiz, J., Demaiffe, D., Weis, D., 1988. Modelling of source enrichment and melting processes for the calc-alkaline–shoshonite–lamproite suite from SE Spain. *Chem. Geol.* 70, 153.
- Hole, M.D., Saunders, A.D., Marriner, G.F., Tarney, J., 1984. Subduction of pelagic sediments: implications for the origin of Ce anomalous basalts from the Mariana Islands. *J. Geol. Soc. (London)* 141, 453–472.
- IGME (Ed.), 1983. *Mapa Sismotectónico de Granada* 1:100,000. Madrid.
- James, D.E., 1981. The combined use of oxygen and radiogenic

- isotopes as indicators of crustal contamination. *Annu. Rev. Earth Planet. Sci.* 9, 311–344.
- Jordan, T.E., Isacks, B.L., Allmendinger, R.W., Brewer, J.A., Ramos, V.A., Ando, C.J., 1983. Andean tectonics related to geometry of subducted Nazca plate. *Bull. Geol. Soc. Am.* 94, 341–361.
- Kay, R.W., Sun, S.S., Lee Hu, C.N., 1978. Pb and Sr isotopes in volcanic rocks from the Aleutian Islands and Pribilof Islands, Alaska. *Geochim. Cosmochim. Acta* 42, 263–273.
- Kogiso, T., Tatsumi, Y., Nakano, S., 1997. Trace element transport during dehydration processes in the subducted oceanic crust: 1. Experiments and implications for the origin of ocean island basalts. *Earth Planet. Sci. Lett.* 148, 193–205.
- Lin, P.-N., 1992. Trace element and isotopic characteristics of western Pacific pelagic sediments: implications for the petrogenesis of Mariana Arc magmas. *Geochim. Cosmochim. Acta* 56, 1641–1654.
- Lonergan, L., Mange-Rajetsky, M.A., 1993. Evidence for internal zone unroofing, Betic Cordillera, SE Spain. In: Séreane, M., Malavielle, J. (Ed.), *Late Orogenic Extension in Mountain Belts*, Vol. 219. Doc. BRGM, p. 126.
- López-Ruiz, J., Rodríguez Badiola, E., 1980. La región volcánica neógena del sureste de España. *Estudios Geol.* 36, 5–63.
- López-Ruiz, J., Wasserman, M.D., 1991. Relación entre la hidratación/desvitrificación y el $\delta^{18}\text{O}$ en las rocas volcánicas neógenas del SE de España. *Estudios Geol.* 47, 3–11.
- López-Ruiz, J., Rodríguez Badiola, E., García Cacho, L., 1977. Origine des grenats des roches calco-alcalines du Sud-Est de l'Espagne. *Bull. Volcanol.* 40, 1–12.
- López-Ruiz, J., Cebriá, J.M., Doblas, M., Oyarzun, R., Hoyos, M., Martín, C., 1993. The late Cenozoic alkaline volcanism of the central Iberian Peninsula (Calatrava Volcanic Province, Spain): intraplate volcanism related to extensional tectonics. *J. Geol. Soc.* 150, 915–922.
- Molin, D., 1980. Le volcanisme miocène du Sud-Est de l'Espagne Provinces de Murcia et d'Almería. PhD Thesis, Univ. Paris VI, 289 pp.
- Morris, J., Tera, F., 1989. ^{10}Be and ^9Be in mineral separates and whole rocks from volcanic arcs: implications for sediments subduction. *Geochim. Cosmochim. Acta* 53, 3197–3206.
- Morris, J., Leeman, W.P., Tera, F., 1990. The subducted component in island arc lavas: constraints from Be isotopes and B–Be systematics. *Nature* 344, 31–36.
- Munksgaard, N.C., 1984. High $\delta^{18}\text{O}$ and possible pre-eruptional Rb–Sr isochrons in cordierite-bearing Neogene volcanics from SE Spain. *Contrib. Mineral. Petrol.* 87, 351–358.
- Munksgaard, N.C., 1985. A non-magmatic origin for compositionally zoned euhedral garnets in silicic Neogene volcanics from SE Spain. *Neues Jahrb. Mineral. Mh.* 2, 73–82.
- Nelson, D.R., 1992. Isotope characteristics of potassic rocks: evidence for the involvement of subducted sediments in magma genesis. *Lithos* 28, 403–420.
- Nelson, D.R., McCulloch, M.T., Sun, S., 1986. The origins of ultrapotassic rocks as inferred from Sr, Nd and Pb isotopes. *Geochim. Cosmochim. Acta* 50, 231–245.
- Nixon, P.H., Thirwall, M.F., Buckley, F., Davies, C.J., 1984. Spanish and Western Australian lamproites: aspects of whole rock geochemistry. In: Kornprobst, J. (Ed.), *Kimberlites and Related Rocks*. Elsevier, Amsterdam, pp. 285–296.
- Nobel, F.A., Andriessen, P.A.M., Hebeda, E.H., Priem, H.N.A., Rondeel, H.E., 1981. Isotopic dating of the post-Alpine Neogene volcanism in the Betic Cordilleras, southern Spain. *Geol. Mijnb.* 60, 209–214.
- Oyarzun, R., Marquez, A., Ortega, L., Lunar, R., Oyarzun, J., 1995. A late Miocene metallogenic province in southeast Spain: atypical Andean-type processes on a smaller scale. *Trans. Inst. Min. Met.* 104, 197–202, Sect. B: Appl. Earth Sci.
- Pearce, J.A., 1982. Trace element characteristics of lavas from destructive plate boundary. In: Thorpe, R.S. (Ed.), *Andesites*. Wiley, New York, pp. 525–548.
- Perfit, M.R., Gust, D.A., Bence, A.E., Arculus, R.J., Taylor, S.R., 1980. Chemical characteristics of island–arc basalts: implications for mantle sources. *Chem. Geol.* 30, 227–256.
- Powell, J.L., Bell, K., 1970. Strontium isotopic studies of alkaline rocks. Localities from Australia, Spain and the western United States. *Contrib. Mineral. Petrol.* 27, 1–10.
- Salvioli, E., Venturelli, G., 1996. Temperature of crystallization and evolution of the Jumilla and Cancarix lamproites (SE Spain) as suggested by melt and solid inclusions in minerals. *Eur. J. Mineral.* 8, 1027–1039.
- Schubert, G., Yuen, D.A., Turcotte, D.L., 1975. Role of phase transitions in a dynamic mantle. *Geophys. J. R. Astron. Soc.* 42, 705–735.
- Taylor, H.P., 1980. The effects of assimilation of country rocks by magmas on $^{18}\text{O}/^{16}\text{O}$ and $^{87}\text{Sr}/^{86}\text{Sr}$ systematics in igneous rocks. *Earth Planet. Sci. Lett.* 47, 243–254.
- Taylor, S.R., McLennan, S.M., 1985. *The Continental Crust: Its Composition and Evolution*. Blackwell, Oxford, 312 pp.
- Taylor, H.P., Sheppard, S.M.F., 1986. *Igneous rocks: I. Processes of isotopic fractionation and isotope systematics*. In: Valley, J.W., Taylor, H.P., O'Neil, J.R. (Eds.), *Stable Isotopes in High Temperature Geological Processes*, Vol. 16. Mineral. Soc. Am. Rev. Mineral., pp. 227–271.
- Thompson, R.N., Morrison, M.A., Hendry, G.L., Parry, S.J., 1984. An assessment of the relative roles of crust and mantle in magma genesis: an elemental approach. *Philos. Trans. R. Soc. London A* 310, 549–590.
- Töksoz, M.N., Minera, J.W., Julian, B.R., 1971. Temperature field and geophysical effects of a downgoing slab. *J. Geophys. Res.* 76, 1113–1138.
- Toscani, L., Venturelli, G., Barbieri, M., Capedri, S., Fernández, J.M., Oddone, M., 1990. Geochemistry and petrogenesis of two-pyroxene andesites from Sierra de Gata, SE Spain. *Mineral. Petrol.* 41, 199–213.
- Toscani, L., Contini, S., Ferrarini, M., 1995. Lamproitic rocks from Cabezo Negro de Zeneta: brown micas as a record of magma mixing. *Mineral. Petrol.* 55, 281–292.
- Venturelli, G., Capedri, S., Di Battistini, G., Crawford, A., Kogarko, L.N., Celestini, S., 1984. The ultrapotassic rocks from southeastern Spain. *Lithos* 17, 37–54.
- Venturelli, G., Mariani, E.S., Foley, S.F., Capedri, S., Crawford, A.J., 1988. Petrogenesis and conditions of crystallization of Spanish lamproitic rocks. *Can. Mineral.* 26, 67–79.
- Venturelli, G., Capedri, S., Barbieri, M., Toscani, L., Salvioli, E.,

- Zerbi, M., 1991. The Jumilla lamproite revisited: a petrological oddity. *Eur. J. Mineral.* 3, 123–145.
- Venturelli, G., Salvioli, E., Toscani, L., Barbieri, M., Gorgoni, C., 1993. Post-magmatic apatite + hematite + carbonate assemblage in the Jumilla lamproites. A fluid inclusion and isotope study. *Lithos* 30, 139–150.
- Vissers, R.L.M., van der Wal, D., 1993. Geology of the Betic lithosphere: evidence for extensional collapse in the Alboran realm. In: Séreane, M., Malavielle, J. (Eds.), *Late Orogenic Extension in Mountain Belts*, Vol. 219. Doc. BRGM, pp. 204–205.
- White, W.M., Dupré, B., 1986. Sediment subduction and magma genesis in the Lesser Antilles: isotopic and trace element constraints. *J. Geophys. Res.* 91, 5927–5941.
- White, W.M., Dupré, B., Vidal, P., 1985. Isotope and trace element geochemistry of sediments from the Barbados Ridge–Demerara Plain region, Atlantic Ocean. *Geochim. Cosmochim. Acta* 49, 1875–1886.
- Woodhead, J.D., 1989. Geochemistry of the Mariana arc (western Pacific): source composition and processes. *Chem. Geol.* 76, 1–24.
- Zeck, H.P., 1968. Anatectic origin and further petrogenesis of almandine-bearing biotite–cordierite–labradorite–dacite with many inclusions of restite and basaltoid material, Cerro del Hoyazo, SE Spain. PhD Thesis, Amsterdam Univ., 161 pp.
- Zeck, H.P., 1970. An Erupted Migmatite from Cerro del Hoyazo, SE Spain. *Contrib. Mineral. Petrol.* 26, 225–246.
- Zeck, H.P., 1992. Restite-melt and mafic–felsic magma mixing and mingling in an S-type dacite, Cerro del Hoyazo, southeastern Spain. *Trans. R. Soc. Edinburgh: Earth Sci.* 83, 139–144.